THESIS

# TEMPERATURE INCREASE MEASUREMENTS OF MULTIPLE 10 ms PULSES OF 2.01 μm LASER LIGHT INCIDENT ON EX-VIVO RABBIT CORNEAS

Submitted by

Edward Kelly

Department of Environmental and Radiological Health Sciences

In partial fulfillment of the requirements

For the Degree of Master of Science

Colorado State University

Fort Collins, Colorado

Summer 2011

Master's Committee:

Advisor: Thomas Johnson

Robert Woody
Alexander Brandl

ABSTRACT

TEMPERATURE INCREASE MEASUREMENTS OF MULTIPLE 10 ms PULSES OF 2.01 μm LASER LIGHT INCIDENT ON EX-VIVO RABBIT CORNEAS

Current laser safety standards for multiple-pulse lasers are based primarily on modeling and the results of single-pulse studies. Previous thermal effects studies have focused on histological and visible endpoints, with only a few studies examining the actual temperatures achieved. The goal of this research was to probe the actual temperature profile produced by 2.01-micron laser pulses in the cornea. In this study the corneal temperature rise from multiple 2.01-micron Tm:YAG laser pulses was investigated using *ex-vivo* rabbit eyes. An infrared thermal camera employing microbolometer detectors captured surface temperature rises resulting from laser pulses. Thermal measurements were taken with single 10-ms pulses as well as two-, three-, and four-pulse sequences while holding the total energy delivered constant for the two- through four-pulse train measurements. An average temperature increase of 8.3 °C was observed with the single pulse at 2.8 J/cm$^2$/pulse irradiance. For two pulses, an average temperature increase of 10.0 °C was observed for 2.7 J/cm$^2$/pulse irradiance. For three pulses, an average temperature increase of 5.8 °C was observed for 1.9 J/cm$^2$/pulse irradiance. For four pulses, an average temperature increase of 4.4 °C was observed for 1.5 J/cm$^2$/pulse irradiance. A comparison of the data to temperatures required for

denaturing proteins and the current laser safety guidelines is presented. It appears that the MPE may be overly conservative by a factor of at least 15. It is recommended that the 2.01-micron laser MPE be investigated to determine if a revision of the standard is warranted.

# ACKNOWLEDGEMENTS

This research and its support were conducted under the guidance of my graduate committee. My advisor, Dr. Tom Johnson, was instrumental in my achieving this study; for all his insight and support, I am forever grateful. I also express many thanks to the other members of my research committee for their support and guidance. Dr. Alex Brandl was very helpful in getting me to clarify important points. Dr. Bob Woody enabled me to see how things look from a different perspective, particularly with the definition of near and far infrared regions.

Many thanks are due as well to Lieutenant Colonel (Dr.) Nick Schaaf, USAF, BSC, whose guidance and assistance with my data collection were invaluable to me. Through him, I came to contact Dr. Robert E. Lee, Biomedical Sciences Coordinator and Erik Themm of Necropsy. These two gentlemen were extremely helpful in providing me with practice eyes at no cost before I obtained the ex-vivo rabbit eyes for my data collection. I thank Dr. Tom Eurell for instructing me in the fine art of slicing frozen tissue and how to properly use a microscope. I would like to express gratitude to Lieutenant Al Riccardi, USN for his help with data collection, his friendship and all his other support along the way as we worked on our degrees. Many thanks to all my Health Physics cohorts for their support and help in course work. And I certainly appreciated all the kind guidance of Ms. Julie Asmus, Ms. Jeanne Brockway and Ms. Aimee Oke.

Finally, I wish to acknowledge the support to my USAF network. Thanks to the program managers at AFIT/CI (particularly Mr. Matt Daniels) and the staff of AFROTC Detachment 90 who have been so helpful. None of this education would have been possible without the help of my former flight commanders Lieutenant Colonel Larry

Calabro, USAF, BSC and Lieutenant Colonel (Retired) Craig Adams, USAF, BSC and former squadron commander Colonel Terry Haske, USAF, MC. Thanks to Colonel Jack Jeter, Colonel, USAF, BSC for selecting me to this AFIT/CI program. To each of these gentlemen, please accept my heartfelt gratitude.

The views expressed in this dissertation are those of the author and do not reflect the official policy or position of the United States Air Force, the Department of Defense, or the U.S. Government.

# DEDICATION

This thesis, all the years of education and all the effort that goes into it, I dedicate to the love of my life – Nancy.

# Contents

# Chapter 1
# Introduction

## 1.1 Introduction

Lasers can potentially produce a non-ionizing radiation hazard within occupational and non-occupational environments. A health physicist is typically the laser safety officer and determines the potential biological effects and operator hazards of lasers which are used in manufacturing processes, optical industries and other operations. Understanding biological effects of lasers enables the health physicist to make educated decisions when evaluating laser hazards and determining safety standards for the organization using the laser. The primary goal of the health physicist is the balance of maximizing laser use while minimizing the risk for health effects associated with non-ionizing radiation in making recommendations and setting standards for the organization using lasers.

Laser safety in the USA is primarily governed by regulations of the U.S. Food and Drug Administration's Center for Devices and Radiological Health (CDRH) and the U.S. Department of Labor's Occupational Safety and Health Administration (OSHA). The CDRH issues many guidance documents for users and manufacturers including laser classification criteria. OSHA implements its regulations concerning lasers, found in 29CFR1910 subpart I, with its standard Guidelines for Laser Safety and Hazard Assessment.[1] The federal regulations of the CDRH concerning lasers are found in 21CFR1040. Both CDRH and OSHA recognize the American National Standards Institute recommendations published in the "Safe Use of Lasers" series of standards in

ANSI Z136.[2] These standards are based on laser health effects, primarily minimal visible lesions, and are used to determine the safety precautions for all types of lasers. These safety standards are directly related to the radiant energy of the laser being used.

### 1.2 Laser Background

The optical laser beam is characterized by six major parameters. These include the duration of irradiation, wavelength, beam diameter and shape, beam divergence, polarization of the light, and the beam's Transverse Electro-Magnetic (TEM) mode(s). The laser beam duration is generally considered to be continuous if it remains on and constant for longer than one quarter second.[2] The beam is considered pulsed if it is on for less than one quarter second, either in a single burst or in a repetitive pattern. The beam wavelength ($\lambda$) is inversely related to the frequency ($f$) by the relationship: $c = \lambda f$ with c representing the speed of light constant. The beam diameter and shape are determined by the gain medium, mirrors, and optical components of the laser.

Most beams have a Gaussian shape in the transverse plane, particularly in low-order TEM modes. A small aperture, in relation to the free running beam size, can produce the "top hat" laser beam shape which approximates a square wave shape. When the beam travels far from the aperture, the top hat beam from this method will return to a Gaussian shape. A "top hat" beam cross section can also be achieved by mixed TEM modes.

The beam radius is usually called the spot size. It is normally reported as the width of the beam at $1/e^2$ of its maximum intensity. In the context of laser safety, a beam size is described at the 1/e intensity level. This provides a margin of safety as the total beam energy is then considered to be concentrated in the smaller area.[2]

The beam divergence is a function of the minimum beam radius and the beam wavelength, before beam focusing with lenses. A laser has the ability to produce a very low rate of beam divergence, but some lasers, such as most diode lasers, produce a very large angle of divergence. The incorporation of a strong lens can overcome this large divergence angle to tighten divergence.

The light from a laser is usually polarized such that it has the orientation of its transverse electric field. Lasers can operate in different TEM modes using different optical cavity configurations. Most commercial lasers operate predominantly in the lowest order – $TEM_{0,0}$ mode. This mode produces the single circular beams familiar today. The lasers used in this study all operated in the $TEM_{0,0}$ mode with a circular shape and Gaussian intensity distribution.

### 1.3 Laser Radiation Interactions with Tissue – Health Physics

Laser radiation can damage tissue regardless if it is in the visible, ultraviolet (UV), or infrared (IR) spectrum. Lasers can deliver enough energy, in such a short time, to living tissue to produce either transient or permanent effects or both. Temporary effects can be induction of pigmentation production and swelling from capillary dilation. Permanent effects include heating, burning, coagulation of blood or proteins, and tissue ablation. A laser's delivery of energy can overwhelm the local tissue's ability to dissipate the heat absorbed.

This study's primary focus is the measurement of thermal energy absorption in the cornea using medium laser power levels with millisecond-scale pulses. The cornea is the part of the eye considered most susceptible to damage from a laser operating at the

2.01-μm wavelength used in this study. Rabbit corneas were used in this study because the rabbit cornea is similar in structure to the human cornea.[3]

Appendix G of ANSI Z136.1[2] describes biological effects of the eye. It describes a minimal corneal lesion as a small white area involving only the epithelium without surface elevation or swelling upon exposure to a laser source. Maximum permissible exposure (MPE) is defined as the exposure limit that is set as a factor of ten above the 50% injury threshold. This threshold is listed in the ANSI standard as the $ED_{50}$, and is the estimated value that results in an injury (not death) 50% of the time. ANSI considers the infrared region as wavelengths from 1.4 to 1000 μm, and states the following. "Excessive infrared exposure causes a loss of transparency or produces a surface irregularity in the cornea. The Maximum Permissible Exposure (MPE) is well below the energy or power required to produce a minimal lesion. These observations are based on experiments with $CO_2$ lasers; extrapolation to wavelengths other than 10.6 μm must be made with care."[2]

The distinction between tissue heating and burning is determined by the rate of heating relative to the rate of heat removal. Studies document tissue damage occurring at lower levels of laser irradiation, rather than burning, since albumins begin to coagulate somewhere between 45º C and 60º C.[4] Modern lasers can deposit energy so quickly that the rapid local temperature rise overwhelms the ability of the local tissue to dissipate the heat. This ultimately can produce injury in the form of burns or other tissue damage.

**1.4 Previous Work**

Many laser systems emit sequences of pulses, but to date, most investigations of corneal damage thresholds for multiple-pulse exposures have been for $CO_2$ laser radiation.[5] Extending investigations of threshold damage for sequences of pulses to more

penetrating wavelengths than 1.4-μm is important, since beyond this wavelength absorption properties of the cornea vary greatly. Such investigations will provide a rational scientific basis for setting laser safety standards.

"The spectral region for wavelengths greater than about 1.4 μm is often called 'eye safe' because the cornea and aqueous humor have sufficient absorption to prevent damaging levels of radiation from reaching the retina. However, because of its absorption, the cornea itself can sustain thermal damage. Much of the work that has been done investigating corneal injury thresholds in the infrared has been for $CO_2$ radiation at 10.6 μm."[5] Radiation at the 1.4-μm wavelength is strongly absorbed, having an absorption depth of about 10 μm, where the absorption depth is the depth at which the irradiance is diminished to 1/e or 37% of its incident level.

The specific laser type of interest in this project provides infrared light at a wavelength of 2.01 microns. The 2.01-micron wavelength is important because it is close to the peak photon absorption in water at 1.94 microns, and the cornea is about 78% water.[3, 6-7] A similar common laser such as the Ho:YAG laser at 2.12 micron wavelength has found popularity in soft tissue medical applications such as urological procedures.[8]

Recently, the introduction of commercially available Tm:YAG lasers at 2.01 micron wavelength has opened even more possibilities for near-infrared laser uses.[9] A thulium-doped fiber laser operating at 2-micron wavelength was first reported in 1990[10] with Jackson and King surpassing the single Watt power output level in a laboratory eight years later.[11] Jackson and King also established the method of adjusting the wavelength of thulium fiber lasers by means of changing fiber length.

Optical properties of the different parts of the eye dictate how much transmission and absorption occurs in tissue.[12] In the infrared wavelength region of the spectrum (1.4 μm to 1 mm), more energy is absorbed by the cornea than is transmitted through to retina and to the back of the eye, so damage occurs at the cornea. Absorbed radiation causes tissue heating and temperature increases disperse to other portions of the eye because of heat conduction. Previous studies showed that over a wide range of exposure durations, corneal cells are damaged when the temperature is raised to about 40°C above ambient (*in-vivo*) cornea temperature.[14] Investigations to date involve corneal damage thresholds for multiple-pulse exposures produced from $CO_2$ laser radiation at 10.6 μm. For widely varying absorption properties of the cornea for wavelengths greater than 1.4 μm, McCally and Bargeron among others investigated threshold damage for sequences of pulses, particularly epithelial damage thresholds for sequences of pulses from a Tm:YAG laser.[4]

### 1.5 Goals of the Study

The primary goal of this study was to measure temperature changes in the cornea resulting from exposure to single and multiple laser pulses to the cornea at a wavelength of 2.01 μm. Current laser safety standards for multiple-pulse lasers are based primarily on modeling and the results of single-pulse studies. Previous thermal effects studies have focused on histological and visible endpoints, with only a few studies examining the actual temperatures achieved.[5] An infrared thermal camera employing microbolometer detectors captured surface temperature increases resulting from laser pulses at the *ex-vivo* rabbit cornea. Single 10-ms pulses as well as two-, three-, and four-pulse sequences were

utilized while the total energy delivered was held constant, except for the single pulse mode because the laser was power constrained and could not deliver this energy.

This study also compared temperature change measurements to theoretical peak temperature calculations. The Tm:YAG threshold peak temperatures were fit by a modified critical peak temperature (CPT) model given by $CPT_{Tm:YAG} = 76D^{-0.054}\,^{\circ}\mathrm{C}$, assuming that the cornea's temperature is 35ºC.[4] The variable *D* describes the pulse train duration: $D = (N-1)/PRF + \tau$, where *N* represents the number of pulses, *PRF* is the pulse recurring frequency and τ is the exposure duration. The McCally and Bergeron study found that threshold damage is correlated by $H_{th} = CN^{-\alpha}$ where $H_{th}$ represents threshold radiant exposure per pulse, *N* is the number of pulses, *C* is a constant depending on the *PRF* and individual pulse duration and the exponent α has a value that can range from 0.22 to 0.29.[5]

# Chapter 2
# Materials and Methods

## 2.1 Industry Standard Laser Alignment Thermal-Sensitive Paper (ZAP-IT paper)

ZAP-IT (Kentek, Pittsfield NH) paper was used to determine the location, beam shape, intensity, divergence and energy distribution of the laser beams. The paper is coated with a proprietary ink sensitive to laser light. When laser light interacts with the paper, the paper responds and is used to determine fluence and data for a non-biological system.

## 2.2 *Ex-vivo* Rabbit Eyes

*Ex-vivo* rabbit eyes were obtained from Pel Freeze (Pel-Freeze Biologicals, Rogers, AR). All rabbit eyes were harvested in a single day and transferred to 4$^{o}$C, F12/DMEM media (MediaTech, Herndon, VA) supplemented with 10% NuSerum (Collaborative Biomedical, Bedford, MA), 2 mM L-glutamine, 500 IU/mL penicillin, 500 µg/mL streptomycin and 1.25µg/mL amphotericin. Eyeballs remained in this solution while shipped via overnight carrier for use. All procedures involving animal tissues were approved under an animal use protocol by the Colorado State University Animal Care and Use Committee.

## 2.3 Laser System

A Newport (Irvine, CA) RS 2000 laser table supported on four Newport RL-2000 series legs was used for positioning all optics including the laser. All exposures were

performed using an IPG Photonics (Oxford, MA) 2.01-μm 50-Watt Thulium YAG Fiber Laser, Model TLM-50-2010 (SN: PL0704233). The main infrared (IR) laser (Thulium YAG laser) was controlled by an IPG Handheld Power Controller (SN: HH342221), allowing the operator to turn the laser on and off, and set laser output power. Pulses for the main laser were generated by providing the laser electronic signals via two frequency generators described below. The fiber optic cable output from the main laser was fixed in position using a Thorlabs (Newton, NJ) C1503 1.5 cm post kinematic V-Clamp mount with two Thorlabs PM1 clamps which attached directly to the V-Clamp.

Pulsing of the main laser was controlled by a Hewlett-Packard (Englewood, CO) Function Generator/Arbitrary waveform generator Model 33120A (SN: US34015616). The frequency generator was set to deliver a 10-ms transistor-to-transistor logic (TTL: 0 – 5 VDC) pulse to trigger the main laser to fire. Two generators were each set to output a 50 Hz square wave, with amplitude of 2.5 Volts, Peak-to-Peak (VPP) which was further offset by 1.25 V in the positive direction. Next, the generator was set to burst mode with one generator triggering the other generator. Burst mode outputs a single pulse from a pulse train when it receives an external trigger in the form of a rising edge of a TTL pulse supplied by the laser operator (described later).

The output of the main IR laser (2.01 μm laser) was made co-linear with a 633-nm HeNe laser (Melles Griot, Albuquerque, NM, Helium Neon laser model 05-LLR-881 (SN: 8273EA)). The HeNe served as a targeting beam and for alignment purposes. A Thorlabs C1503 1.5 cm post kinematic V-Clamp mount with two Thorlabs PM1s as the clamps held the HeNe laser in place. The HeNe and the main IR beam were set up perpendicular to one another with a beam combiner placed at their intersection. A

Thorlabs kinematic mount for thin 2 cm optics (model KM200T) held the beam combiner (Thorlabs 2 cm cold mirror with an angle of incidence of 45°, model FM203) in place. The cold mirror provided a transmissive path for the main 2.01-μm IR beam while reflecting the 633 nm HeNe. It was positioned in such a way that the two beams overlap after reflection and transmission with average reflectivity greater than 98% from 1 μm to 5 μm. The HeNe beam was essential to the laser operator for aiming the beam.

Alignment was established by removing the first gold mirror so the beam could travel over 3 meters to a wall. Coincidence of the red HeNe and the invisible Tm:YAG beams was found with commercial thermally active Zap-It paper (Kentek, Pittsfield, NH) by ensuring that the marked produced by the Tm:YAG-emitted laser lined up with the HeNe laser on the paper. This HeNe laser was selected in part for the low divergence of its beam at 1.7 mrad in the far field.

Once the HeNe was co-linear with the main beam, a portion of the two beams was sampled, taking a certain fraction of the beam and directing it to an energy-measuring probe. Sampling allowed determination of the energy of an *ex-vivo* rabbit cornea's exposure via a conversion factor. Since the sampling process takes a fixed portion of the beam, if a given energy is read out on the sampling probe it can be converted to determine how much energy was delivered to the subject corneas.

Energy was sampled using a Thorlabs Pellicle Beamsplitter model BP208. The beamsplitter is uncoated with a reflectance/transmission of 9/92% for 0.400-2.4 μm at 45° angle of incidence (AOI). The beamsplitter was held in place by a Thorlabs 2 cm Fixed Pellicle Mount model BP207. The reflected beams were sent to a Coherent (Santa

Clara, CA) Power Sensor Model PM10 (SN: 8632) with an EPM 2000 dual-channel power meter (SN: 0668E07) set to integrate mode for energy readout. The EPM 2000 was also wavelength-adjusted to 2.01 μm.

The co-linear beams were directed to the subject by an articulated arm (Laser Mechanisms, Inc, Farmington Hills, MI). The lasers were first directed to an adjustable beam bender launch assembly (Model: PLBBA0001) which housed a block bender mount (Model: PLAMH0018). Attached to the top of the block bender mount was a seven-knuckled articulated arm assembly (Model: PLATA0428). The arm was counterbalanced by an articulated arm counter weight (Model: PLATW0002). The mirrors in the knuckles were employed gold mirrors, 1 cm diameter, 0.375 cm thick (Model: PG-PM-1037-C). This arm allowed both the visible and IR beams to be directed to the measurement site safely. A schematic of the setup is shown in Figure 2.1, and Figures 2.2 through 2.7 display selected pictures that show equipment and setup. Appendix A presents engineering drawings of various components of the experimental setup. This appendix also provides equipment set-up information for future studies.

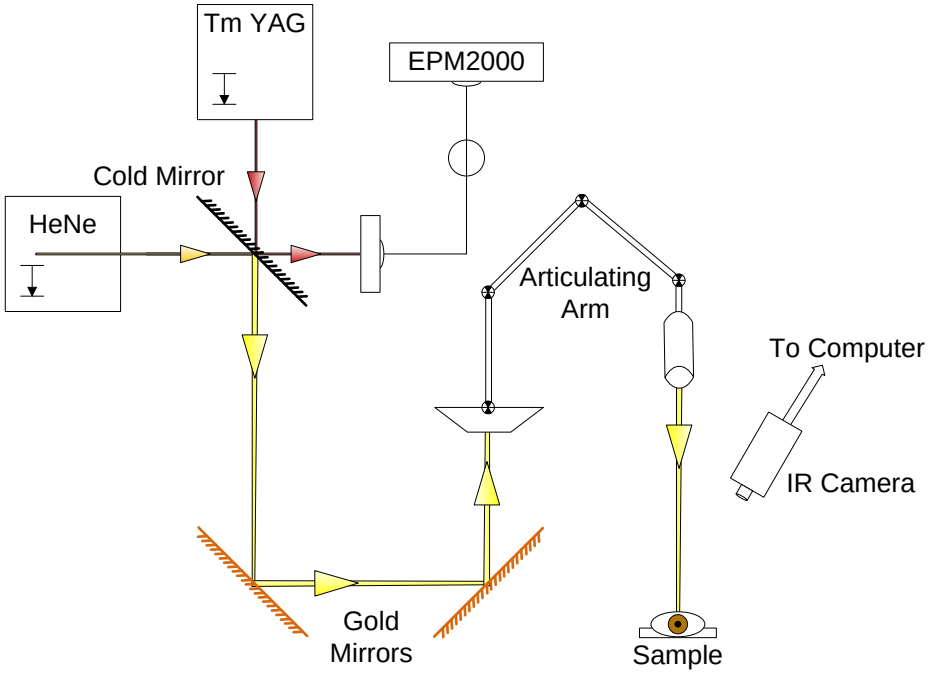


Figure 2.1. Laser schematic showing the optics path. IR beam is red, HeNe positioning beam is orange. The "Cold Mirror" is highly reflective to visible light while transparent (>98% transmission) to IR. The small reflection is measured by the PM10 probe with the EPM2000 meter to record the exposure energy of each irradiation.

An additional Coherent Power Sensor (Model: PM10-V1 SN: 8837) was used to measure the main beams output. This was also attached to the EMP 2000, again set to integrate mode and wavelength corrected for 2.01 µm.

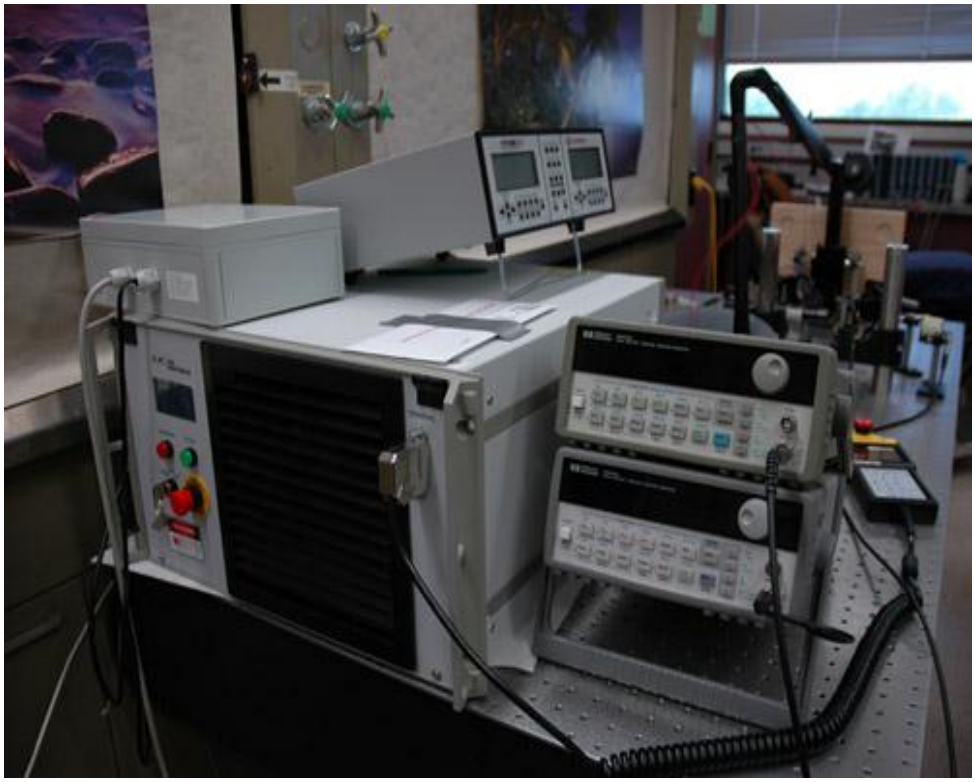

Figure 2.2. Laser and instrumentation setup. The IPG Photonics laser is the largest case on the lower left. Above it, a safety interlock sits atop the laser, and the EPM2000 integrating power meter sits to the rear of the laser. Two Hewlett-Packard waveform generators are shown to the right of the laser.

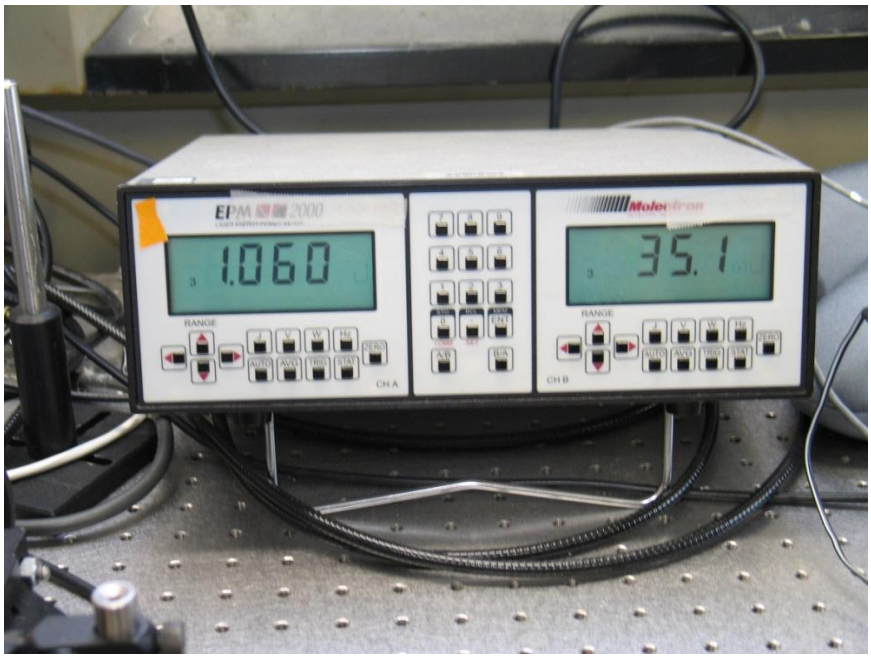


Figure 2.3. The EPM2000 Integrating Power Meter is shown.

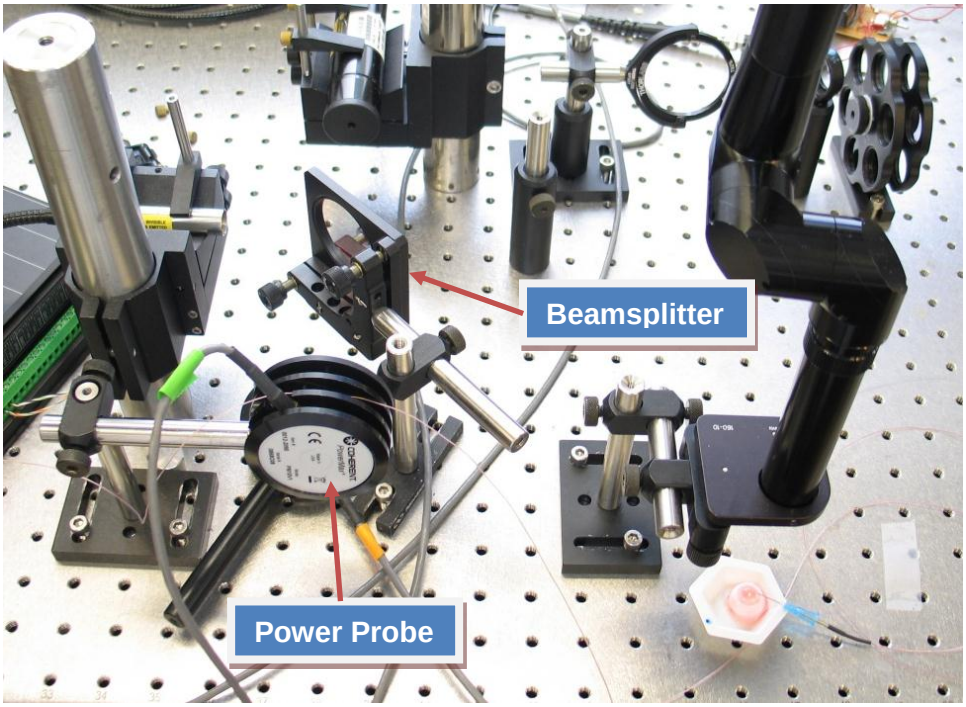


Figure 2.4. The laser setup. The Tm:YAG laser is shown on the left with HeNe shown on top. Figure 2.5 shows this positioning more clearly. On the bottom left center, a beamsplitter and EPM2000 power probe. On the right, the sample eye received laser energy exiting the articulating arm. A thermocouple was inserted in the eye that measured temperature increases, but was not included in this study.

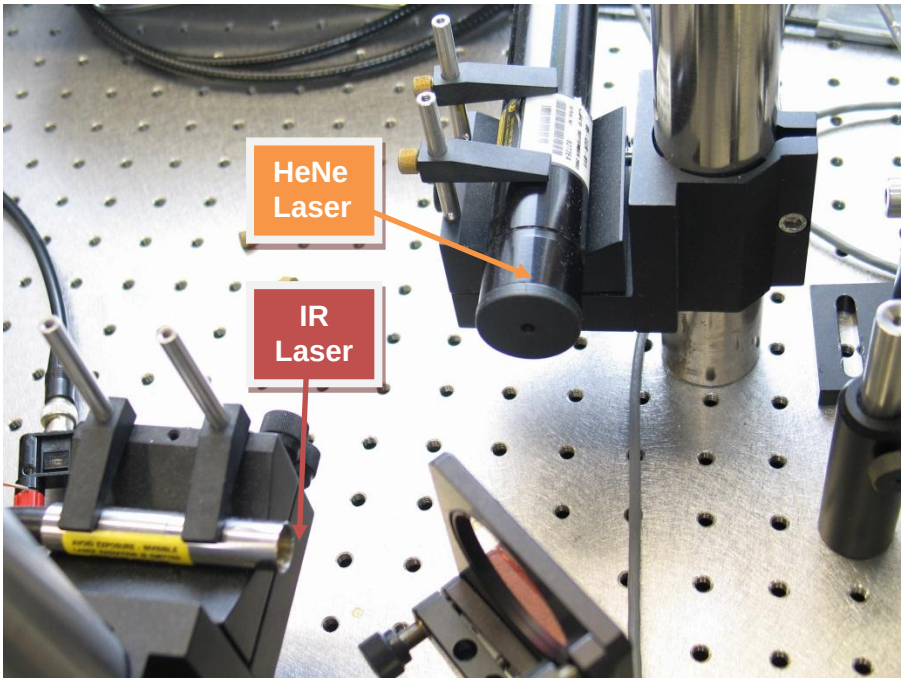


Figure 2.5. Close-up look of the two lasers and the cold mirror.

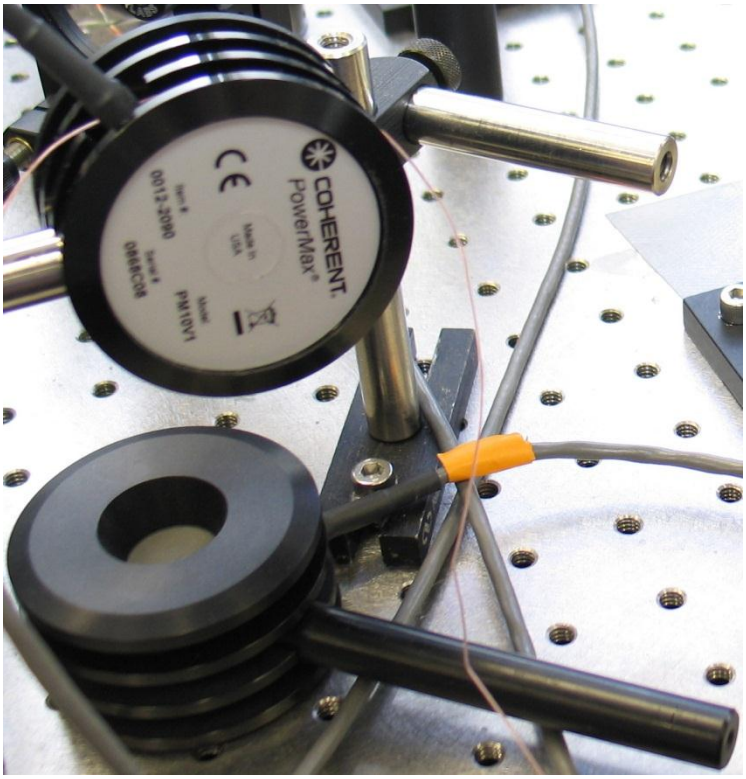


Figure 2.6. Two sides of the EPM2000 power sensor.

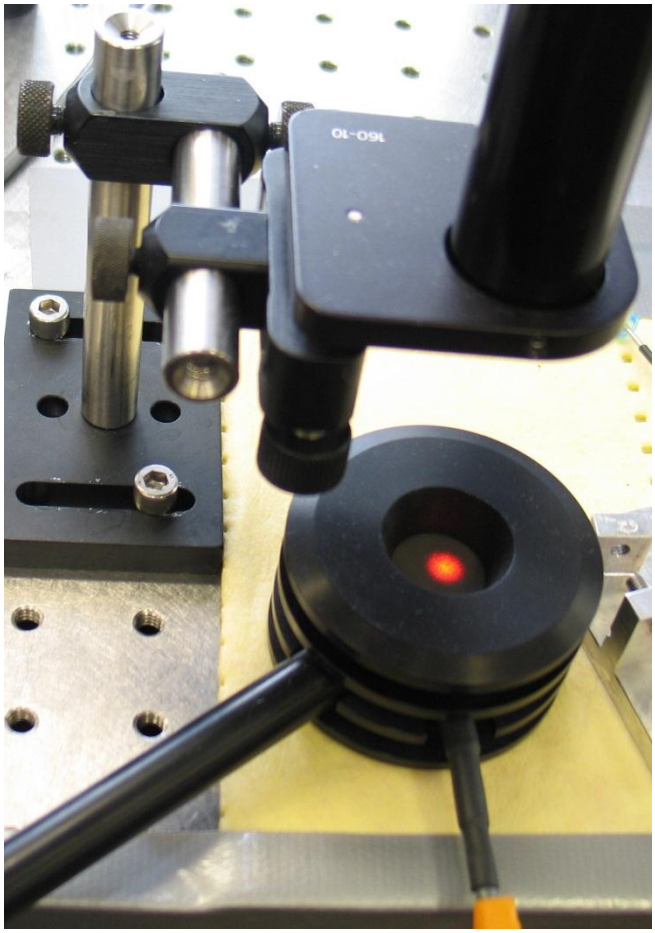

Figure 2.7. The visible HeNe output shows how beam energy exiting the articulating arm was measured.

## 2.4 Power and Beam Width Measurements

The IR beam reflected by the HeNe alignment mirror was measured and recorded for each sample exposed. The IR laser output from the articulating arm was calibrated to the split beam sample prior to each exposure session. The beam probes were PM10 air-cooled thermopile sensors (Coherent, Santa Clara CA) calibrated by the manufacturer with an uncertainty of ± 1%. The sensors were read by an EPM2000 model meter (Coherent, Santa Clara, CA). The meter was also calibrated by the manufacturer with a stated uncertainty of ± 0.03% of full scale reading.

The IR beam incident on the sample had a Gaussian shape with a measured 3.3 mm $1/e^2$ radius using a pinhole technique in both directions.[16] Beam shape was confirmed to be uniform, circular in the lowest order TEM mode, and aligned with the HeNe beam with Zap-It thermal paper prior to each measurement session. Exposures were made on the thermal paper prior to the beam entering the armature and after the beam exited the armature at the location of the cornea sample. The thermal paper impressions were then visually compared to previous sessions' marks to identify any changes. The thermal paper exposures were performed with the laser to assure identical beam patterns both entering and exiting the articulating arm with the same laser settings.

### 2.5 Irradiation and Measurement

Four different pulse sequences were used to irradiate the rabbit corneas. The first was a single 10-ms pulse. The remaining sequences were two 10-ms pulses (duty factor 0.08 of the 250 m period), three 10-ms pulses (duty factor 0.12), and four 10-ms pulses (duty factor 0.16). As previously stated, the 2.01-μm wavelength laser beam had a $1/e^2$ radius of 3.3 mm as measured with a pin-hole method to obtain the beam width.

### 2.6 Thermal Camera

A thermal camera was used to measure the surface temperature change during irradiation and cooling after irradiation. The non-contact thermal imaging FLIR Systems IR Camera (Boston, MA, Model: TheramCAMS65 SN: 21803885) was mounted on a Davis and Sanford camera tripod (The Tiffen Co, Rochester, NY, Model: Magnum X3T Tripod) and interfaced to a Dell LATITUDE D620 computer via a firewire (IEEE 1394) cable. The computer allowed for camera control and data collection. The camera was positioned approximately one meter from sample cornea.

The camera's detector was a 320 × 240 array of micro-bolometer elements. The camera was calibrated by the manufacturer with a sensitivity specification of ± 0.05 ºC with NIST-traceable blackbody sources. The micro-bolometer responds to infrared radiation in the spectral range of 7.5 to 13 μm with a change in resistance to applied bias. The thermal camera was mounted on a secure tripod at one meter from the rabbit eye at an angle of approximately 30º off of normal. The raw data were extracted from the thermal images using the manufacturer's software, Researcher Pro version 2.8 (FLIR Systems, Wiesbaden, Germany).

# Chapter 3
# Data and Analysis

## 3.1 Pulse Set-Up and Initial Measurements

Two signal generators controlled the laser pulsing. A 10-ms pulse-width TTL (transistor-to-transistor logic) signal drove the laser output pulse(s). Refer to Figure 3.1 through Figure 3.4 for oscilloscope-captured plots for 1, 2, 3 and 4 pulses of the laser-pulse setup. The total time of all pulsing was 250 ms. The time interval between rising edges for each pulse of a two-pulse train was 240 ms, and this interval was used to complete all pulses within a 250 ms time interval. A 250 ms interval was used for 3 and 4 pulses as well. To enable the laser, the TTL voltage-level requirement for a logic (High) level was a voltage greater than 2.7 Volts.[17] The laser was considered continuous wave (CW) for pulse durations ≥ 250 ms.[2]

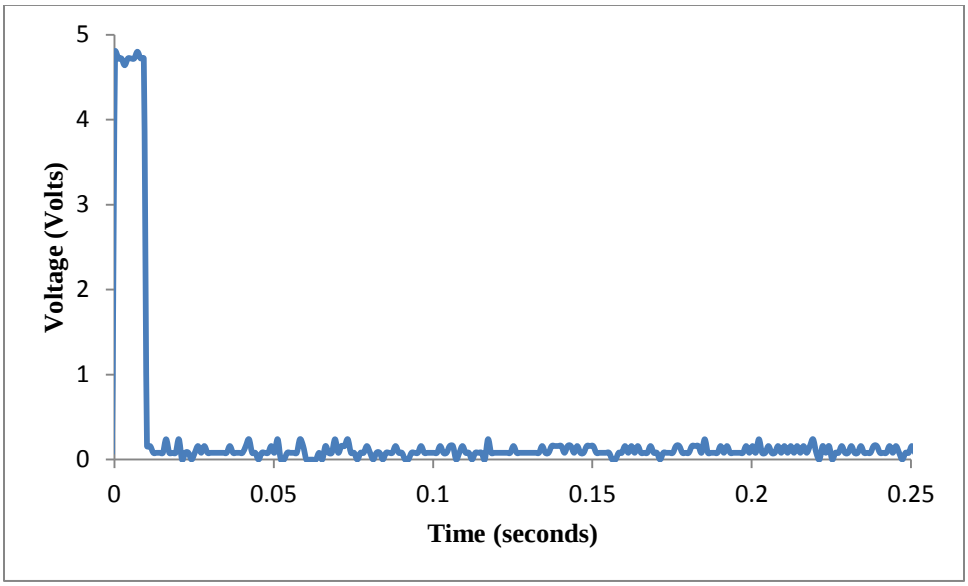

Figure 3.1. Pulse triggering for the laser for a single pulse. Pulse duration was 10 ms.

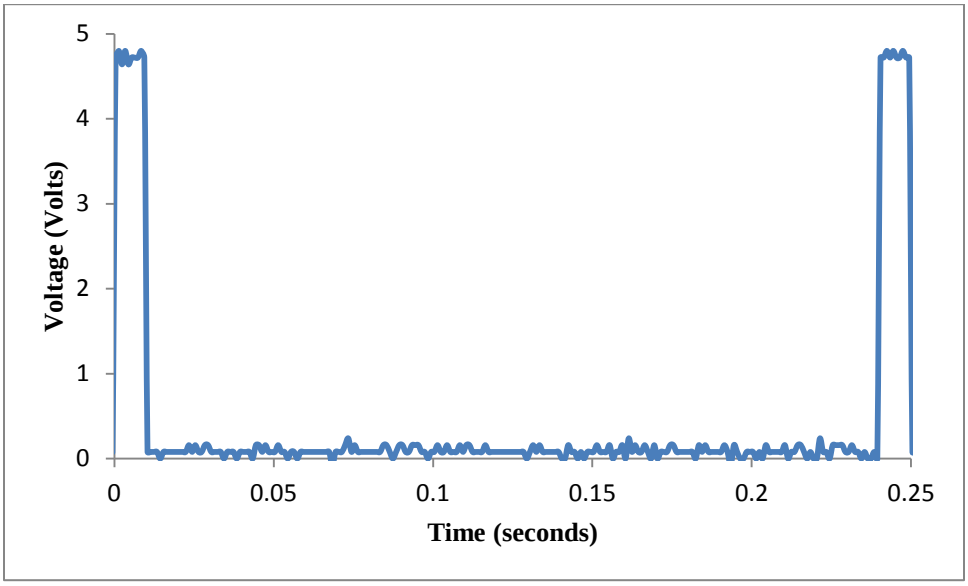


Figure 3.2. Pulse triggering for the laser for two pulses. Pulse duration was 10 ms. The rising edge time between pulses was 240 ms.

The rising edge time between the three pulse train was 120 ms. The four pulse train had 80 ms between the rising edges of the pulses.

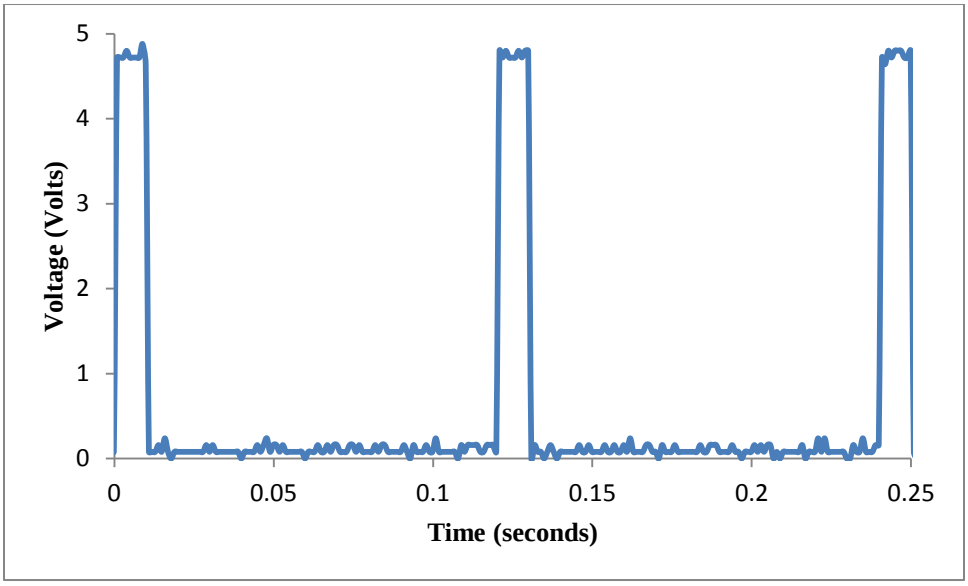

Figure 3.3. Pulse triggering for the laser for three pulses. Pulse duration was 10 ms.
The rising edge time between pulses was 120 ms.

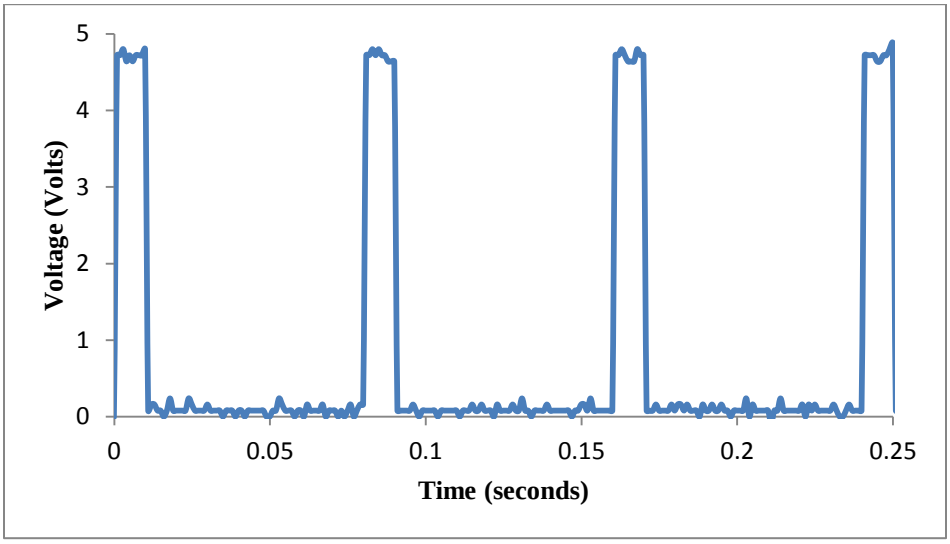


Figure 3.4. Pulse triggering for the laser for four pulses. Pulse duration was 10 ms.
The rising edge time between pulses was 80 ms.

Power was adjusted to obtain an energy irradiance of equivalent levels for each number of pulses delivered to the *ex-vivo* rabbit cornea with the laser set up for a pulse width of 10 ms. The laser was set to a maximum of 100% power with the energy of 459 mJ as measured using the EPM 2000 power meter in integrate mode for a single pulse. The laser was set to 100% with the total measured energy at 899 mJ for two pulses. Three pulses with power at 75% obtained a measured 969 mJ. Four pulses delivered a total of 967 mJ with the laser power level set to 60%. Refer to Table 3.1 below for details of the different pulse trains including maximum permissible exposure (MPE).

| Number of Pulses | 1 | 2 | 3 | 4 |
|---|---|---|---|---|
| **Power %** | 100 % | 100 % | 75 % | 60 % |
| **Total Energy** | 459 mJ | 899 mJ | 969 mJ | 967 mJ |
| **Beam Width (1/e)** | 0.23 cm | 0.23 cm | 0.23 cm | 0.23 cm |
| **Irradiance (H)** | 2.76 J/cm$^2$ | 5.41 J/cm$^2$ | 5.83 J/cm$^2$ | 5.82 J/cm$^2$ |
| **MPE Rule 1** | 0.177 J/cm$^2$ | 0.211 J/cm$^2$ | 0.233 J/cm$^2$ | 0.250 J/cm$^2$ |
| **MPE Rule 2** | 0.396 J/cm$^2$ | 0.198 J/cm$^2$ | 0.132 J/cm$^2$ | 0.099 J/cm$^2$ |
| **MPE Rule 3** | 0.177 J/cm$^2$ | 0.149 J/cm$^2$ | 0.135 J/cm$^2$ | 0.125 J/cm$^2$ |
| **MPE** | 0.177 J/cm$^2$ | 0.149 J/cm$^2$ | 0.132 J/cm$^2$ | 0.099 J/cm$^2$ |

Table 3.1. Laser set up and measurements. Calculated irradiance and MPE are listed too.

The beam width radius is shown in Table 3.1. ANSI Z136.1-2007[2] uses the 1/e measurement for all calculations. Irradiance is calculated using the formula:

$$H = E / (\pi r^2) \qquad \text{Eq. (1)}$$

Table 3.1 provides the calculated irradiance for each of the sets of data for the different pulse trains emitted from the laser. The irradiance calculation is computed by dividing the incident power by the area of the laser beam using the beam width radius as described above in Eq. (1). Sometimes it is desirable to use the $1/e^2$ radius rather than the 1/e radius. Specifically, the military uses the $1/e^2$ radius. The relationship between these 2 radii is that the 1/e radius is calculated by

$$r_{(1/e)} = r_{(1/e^2)} / \sqrt{2} \qquad \text{Eq. (2)}$$

The MPE was calculated using ANSI Z136.1-2007 (Table 5a)[2] at 2.01 μm wavelength. Table 3.1 lists the different pulse MPEs for each of the three rules from ANSI Z136.1-2007. The smallest value is the most restrictive and is used as the MPE.

The formula for the single pulse (Rule 1) is

$$\text{MPE} = 0.56t^{0.25} \qquad \text{Eq. (3)}$$

with the time of exposure ($t$) found by the emitted laser pulse width.

For Rule 2, the potential exposure for all exposure durations, $T$, less than or equal to $T_{max}$ is compared with the MPE for $T$ with the corresponding limiting aperture determined from $T$.[2] The formula used Eq. (3) with $t$ = 0.25 s, divided by the number of pulses (# pulses). In other words,

$$\text{MPE} = \frac{0.56t^{0.25}}{\#\ pulses}, \text{where \# pulses} = 1,2,3,4 \qquad \text{Eq. (4)}$$

For Rule 3, the aperture is determined from the duration of a single pulse ($\leq$ 0.25 s). The energy from a group of pulses with an inter-pulse spacing of $t_{min}$ or less is considered a single pulse for Rule 3.[2] The formula used the single pulse of Eq. (3) and multiplied it by the # pulses raised to the -0.25 power as listed in Eq. (5).

$$\text{MPE} = 0.56t^{0.25} \times \#\ pulses^{-0.25}$$

Eq. (5)

Comparing the appropriate MPE with the different irradiances calculated, the MPE is exceeded in each case.

Refer to Figure 3.5 for the block diagram of the experimental setup. A reflected energy measurement was taken from the first mirror (left mirror shown in Figure 3.5). An energy measurement was taken at the location where each *ex-vivo* rabbit cornea sample

location along with the reflected energy. The EPM 2000 power meter was operated in integrate mode to concurrently capture this energy and the incident energy was measured at the *ex-vivo* rabbit cornea location (marked "Sample" on Figure 3.5). A reflected energy measurement was taken for each set of pulses when each *ex-vivo* rabbit cornea was exposed to the laser emission. The reflected energy provided an indication that the *ex-vivo* rabbit cornea was exposed to the laser, as well as measured a fraction of energy to ascertain the delivered energy for each pulse train.

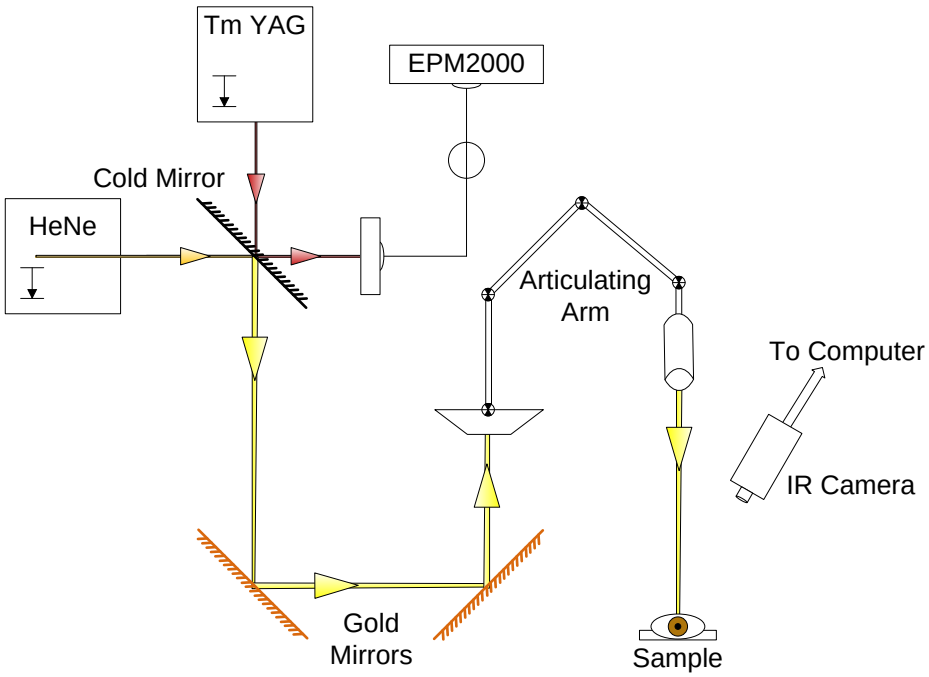


Figure 3.5 (reproduced from Figure 2.2 for convenience). Laser schematic showing the optics path, IR beam is red, HeNe positioning beam is orange. The "Cold Mirror" is highly reflective to visible light while transparent (>98% transmission) to IR. The small reflection is measured by the PM10 probe with the EPM2000 meter to record the exposure energy of each irradiation.

Table 3.2 below lists the averages and standard deviations for each set of data.

| Reflected Energy (mJ) | 1 Pulse | 2 Pulses | 3 Pulses | 4 Pulses |
|---|---|---|---|---|
| **Average** | 32.7 | 62.6 | 63.1 | 59.7 |
| **Standard Deviation** | 3.0 | 7.0 | 4.3 | 3.7 |

Table 3.2. Statistics for reflected energy of laser emission incident on rabbit eyes.

### 3.2 Beam Area Measurements

The $1/e^2$ beam-width radius was obtained using the pin-hole method outlined in ANSI Z136.4-2005[2], and was 0.33 cm. Refer to Figure 3.6 below for a plot of measurements taken for the pin-hole method. Measurements began by first finding the maximum energy peak. Once the maximum energy peak was found, other energy data points were measured in two orthogonal directions off of this peak energy.

The orthogonal measurements using (relative) compass headings were used to illustrate the two axes of the 3-D data in 2-D, so N-S refers to north-south while E-W refers to east-west. The measurements were normalized, and a Gaussian fit was applied to the measured normalized data. The dashed lines in the plot show the points taken from the Gaussian fit curves to determine this beam radius. Then, the area is simply calculated from the obtained radius ($r$) into the area of a circle equation, $A = \pi r^2$.

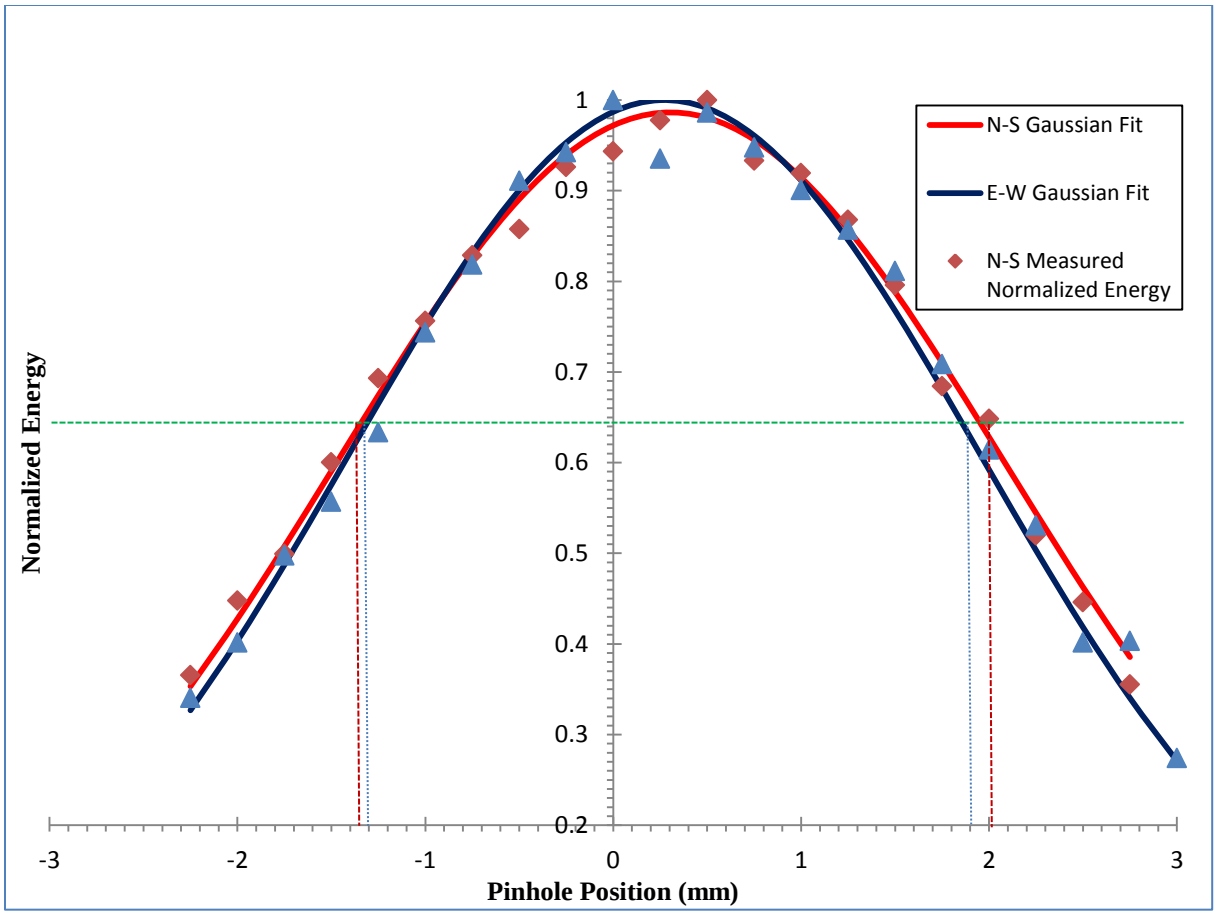


Figure 3.6. Pin-hole method fit to obtain a beam (width) radius fit profile used to determine laser area.

### 3.3 Single Pulse

Single-pulse measurements with the FLIR camera software yielded a average maximum temperature of 25.8 °C and standard deviation of 2.2 °C and an average temperature increase () of 8.2 °C with standard deviation of 2.6 °C. The overall maximum temperature was 30.3 °C with a maximum ΔT of 12.2 °C.

An example of the FLIR camera display is seen by referring to Figure 3.7.

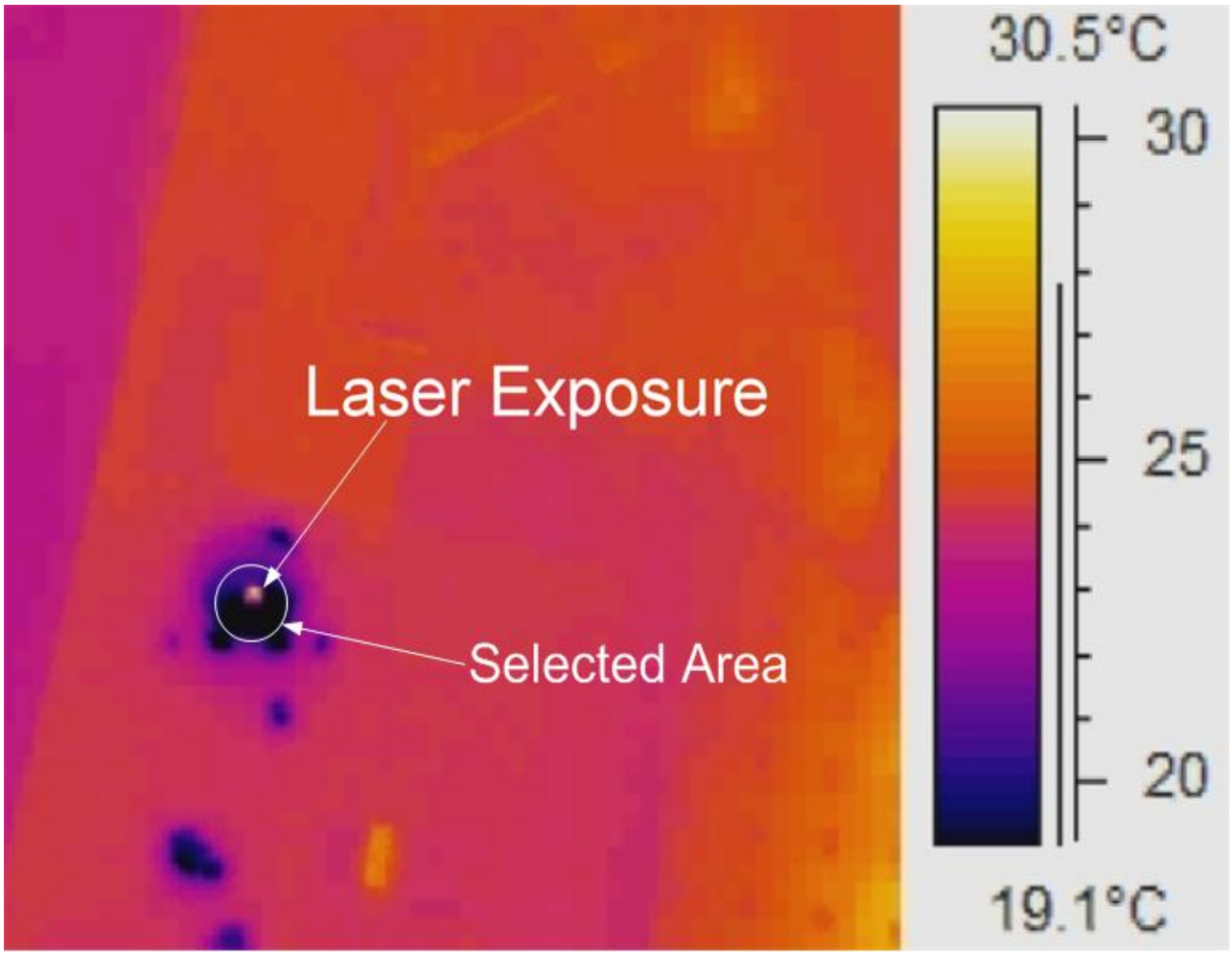


Figure 3.7. Captured image of a FLIR camera frame. The red spot pointed out by the arrow marked "Laser Exposure" shows where in the eye exposure occurred. The dark black spot is where the eye pupil is located. The "Selected Area" is the area used by the software to produce temperature data.

Normalized data was derived using the FLIR camera software to obtain the maximum temperature readings within the area that was selected. In Figure 3.7, this area is represented by "Selected Area" on the figure. Data was collected for 16 different exposures for the single pulse measurements. A plot of overlaying exposures of these single-pulse measurements is in Figure 3.8.

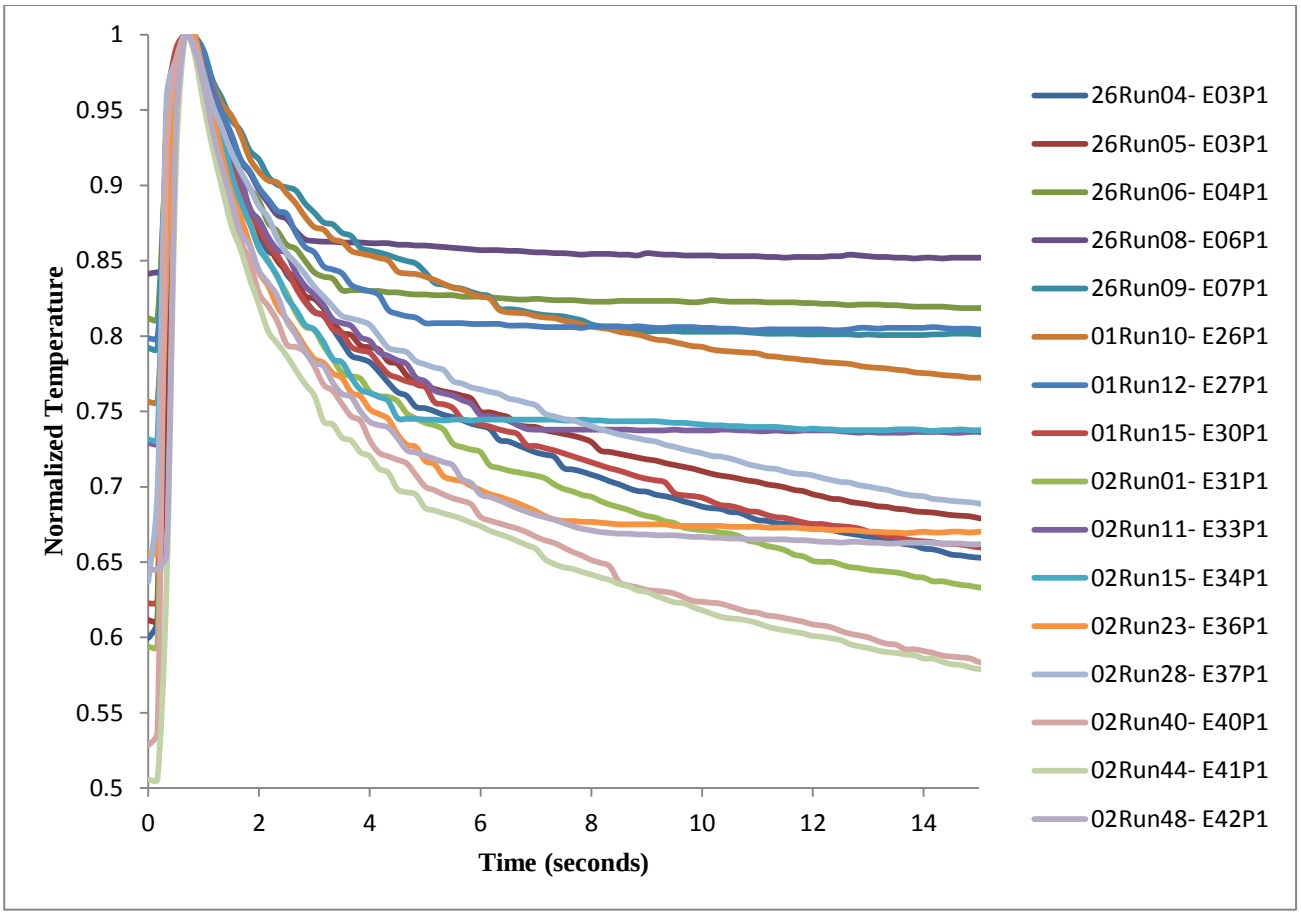


Figure 3.8. Normalized data for single-pulse exposures for 16 separate data runs. The legend is defined in Appendix B.

An ensemble averaging the 16 eye exposures was used to generate a single plot to consolidate these separate runs to a single plot. A plot displaying this averaging can be seen by referring to Figure 3.9. The temperature essentially returns to the baseline in about 11 seconds using a qualitative visual assessment. Table 3.3 summarizes statistics for each of the pulse trains.

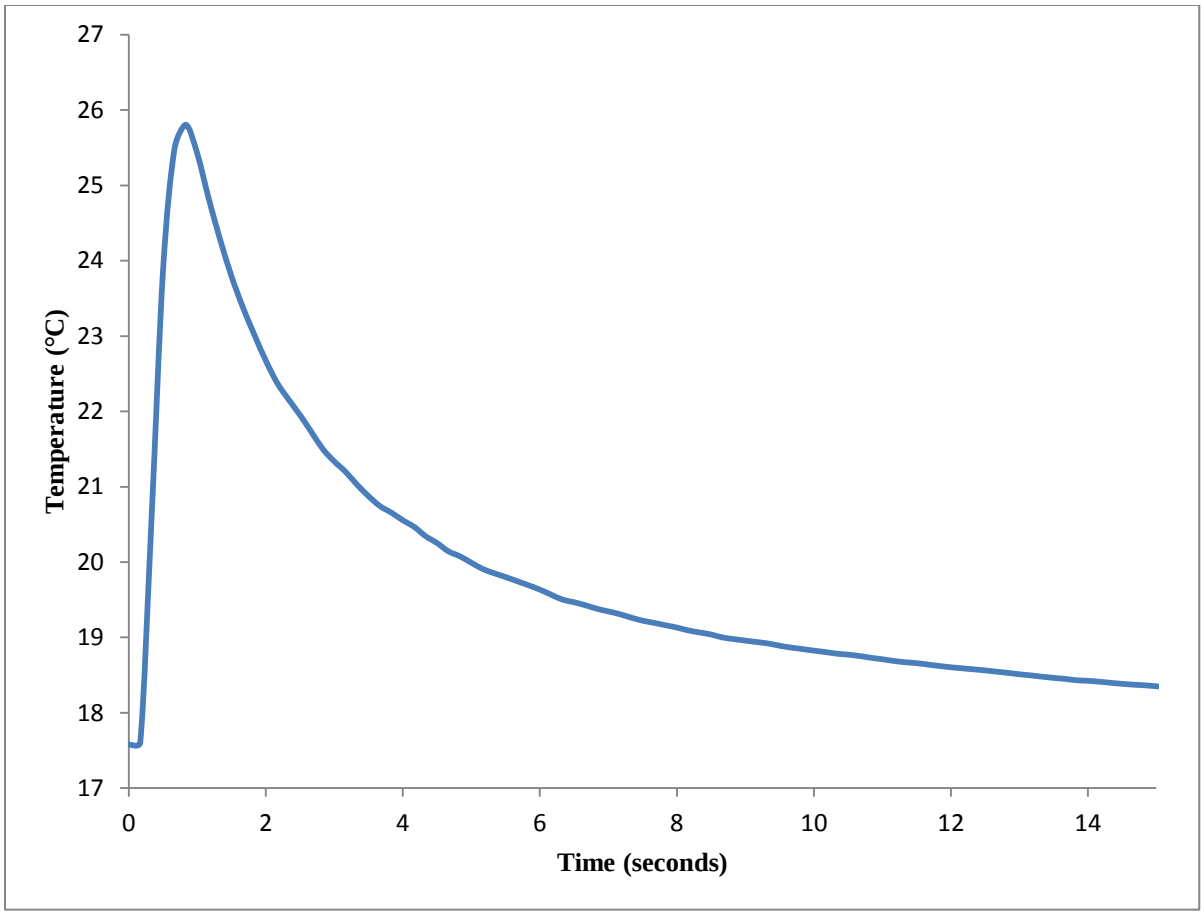


Figure 3.9. Ensemble averaging of 16 eye exposures of temperature over time with a single laser pulse, incident energy at 2.76 J/cm$^2$.

| # Pulses | Avg Max T (°C) | StDev Max T (°C) | Avg T Increase (°C) | StDev Avg T Increase (°C) | Overall Max T (°C) | Max ΔT (°C) | Base T (°C) | Time to Return to Baseline (s) |
|---|---|---|---|---|---|---|---|---|
| 1 | 25.8 | 2.2 | 8.3 | 2.6 | 30.3 | 12.4 | 17.6 | 11 |
| 2 | 33.0 | 1.9 | 16.5 | 1.3 | 36.4 | 18.4 | 16.5 | 19 |
| 3 | 35.5 | 1.9 | 17.0 | 1.8 | 38.3 | 20.0 | 18.6 | 25 |
| 4 | 36.0 | 1.7 | 17.7 | 1.5 | 39.6 | 19.9 | 18.3 | 33.5 |

Table 3.3. Pulse train statistics for temperature (T) changes.

Table 3.4 lists temperature changes per irradiance and Table 3.5 lists temperature rise and fall rates between pulses. The fall times in Table 3.5 do not have the last pulse fall time because this time is incorporated into the time to return to baseline listed in the last

column of Table 3.3. The return to baseline was determined by a visual assessment because the starting temperature of the *ex-vivo* rabbit cornea was colder than room temperature.

| # Pulses | 1st Pulse ΔT/H (°C·cm²/J) | 2nd Pulse ΔT/H (°C·cm²/J) | 3rd Pulse ΔT/H (°C·cm²/J) | 4th Pulse ΔT/H (°C·cm²/J) |
|---|---|---|---|---|
| 1 | 3.0 | | | |
| 2 | 3.5 | 4.0 | | |
| 3 | 2.9 | 3.3 | 2.8 | |
| 4 | 3.0 | 3.6 | 3.1 | 2.6 |

Table 3.4. Temperature change data per irradiance.

| # Pulses | 1st Pulse rising edge (°C/s) | 2nd Pulse rising edge (°C/s) | 3rd Pulse rising edge (°C/s) | 4th Pulse rising edge (°C/s) | 1st Pulse falling edge (°C/s) | 2nd Pulse falling edge (°C/s) | 3rd Pulse falling edge (°C/s) |
|---|---|---|---|---|---|---|---|
| 1 | 9.9 | | | | | | |
| 2 | 14.2 | 12.8 | | | -2.3 | | |
| 3 | 6.8 | 7.7 | 6.4 | | -0.9 | -2.3 | |
| 4 | 6.5 | 10.5 | 8.9 | 5.6 | -0.0 | -0.3 | -0.8 |

Table 3.5. Temperature rate change (rising and falling).

### 3.4 Two Pulses

Two-pulse measurements with the FLIR camera yielded an average temperature maximum of 33.0 °C and standard deviation of 1.9 °C and an average temperature increase of 16.5 °C with standard deviation of 1.3 °C (see Table 3.3). The overall maximum temperature was 36.4 °C with a maximum temperature increase of 18.4 °C. The total irradiance was 5.41 J/cm$^2$ with a ΔT/H of 3.5 °C·cm$^2$/J for the first pulse and 4.0 °C·cm$^2$/J for the second pulse. (See Table 3.4.)

Normalized data was derived using the FLIR camera software to obtain the maximum temperature readings, and this data is shown in Figure 3.10. Data was collected for 13 different exposures, and Figure 3.10 also shows overlaying exposures.

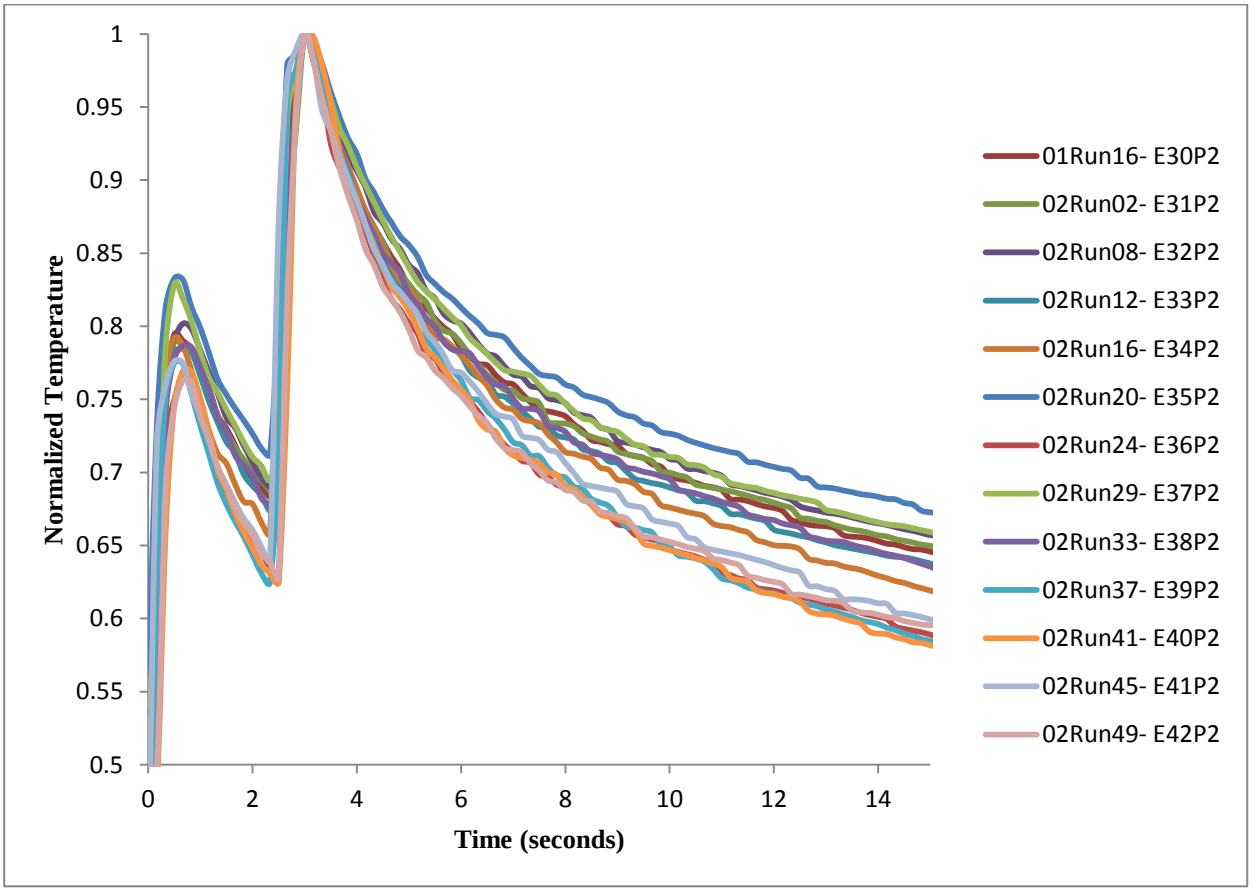


Figure 3.10. Normalized data for two-pulse exposures for 13 separate data runs. The legend is defined in Appendix B.

An ensemble averaging 13 eye exposures was used to generate a single plot to consolidate these separate runs to a single plot. A plot displaying this averaging can be seen by referring to Figure 3.11. The temperature essentially returns to the baseline in about 19 seconds. Table 3.3 summarizes statistics for each of the pulse trains. Table 3.5 lists rise and fall $\Delta T/\Delta t$ rates.

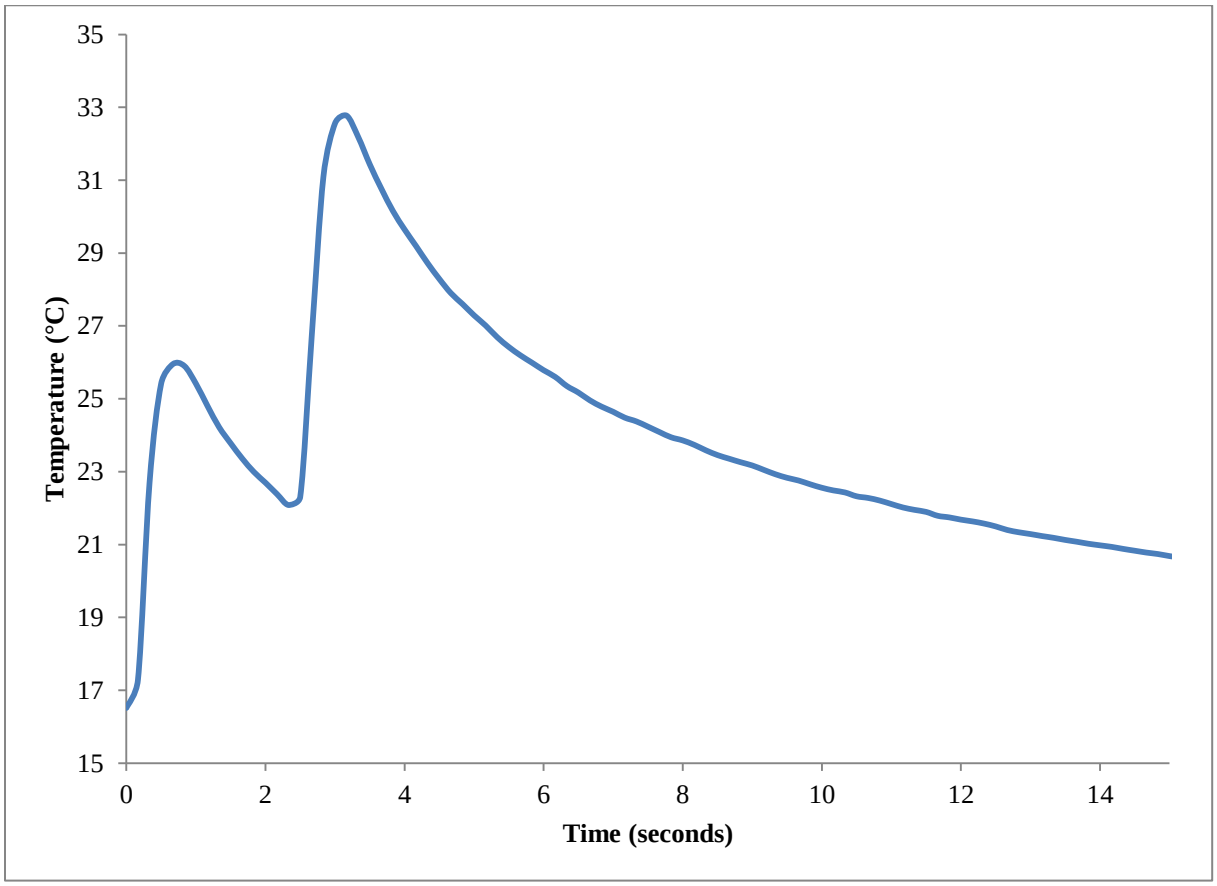


Figure 3.11. Ensemble averaging of 13 eye exposures of temperature over time with two laser pulses, incident energy at 5.41 J/cm$^2$.

### 3.5 Three Pulses

Three-pulse measurements with the FLIR camera yielded an average temperature maximum of 35.5 °C and standard deviation of 1.9 °C and an average temperature increase of 17.0 °C with standard deviation of 1.8 °C. (See Table 3.3.) The overall maximum temperature was 38.3 °C with a maximum temperature increase of 20.0 °C. The total irradiance was 5.83 J/cm$^2$ with a $\Delta T/H$ of 2.9 °C·cm$^2$/J for the first pulse, 3.3 °C·cm$^2$/J for the second pulse and 2.8 °C·cm$^2$/J for the third pulse. (See Table 3.4.)

Normalized data was derived using the FLIR camera software to obtain the maximum temperature readings, and this data is shown in Figure 3.12. Data was collected for 15 different exposures, and Figure 3.12 shows overlaying exposures.

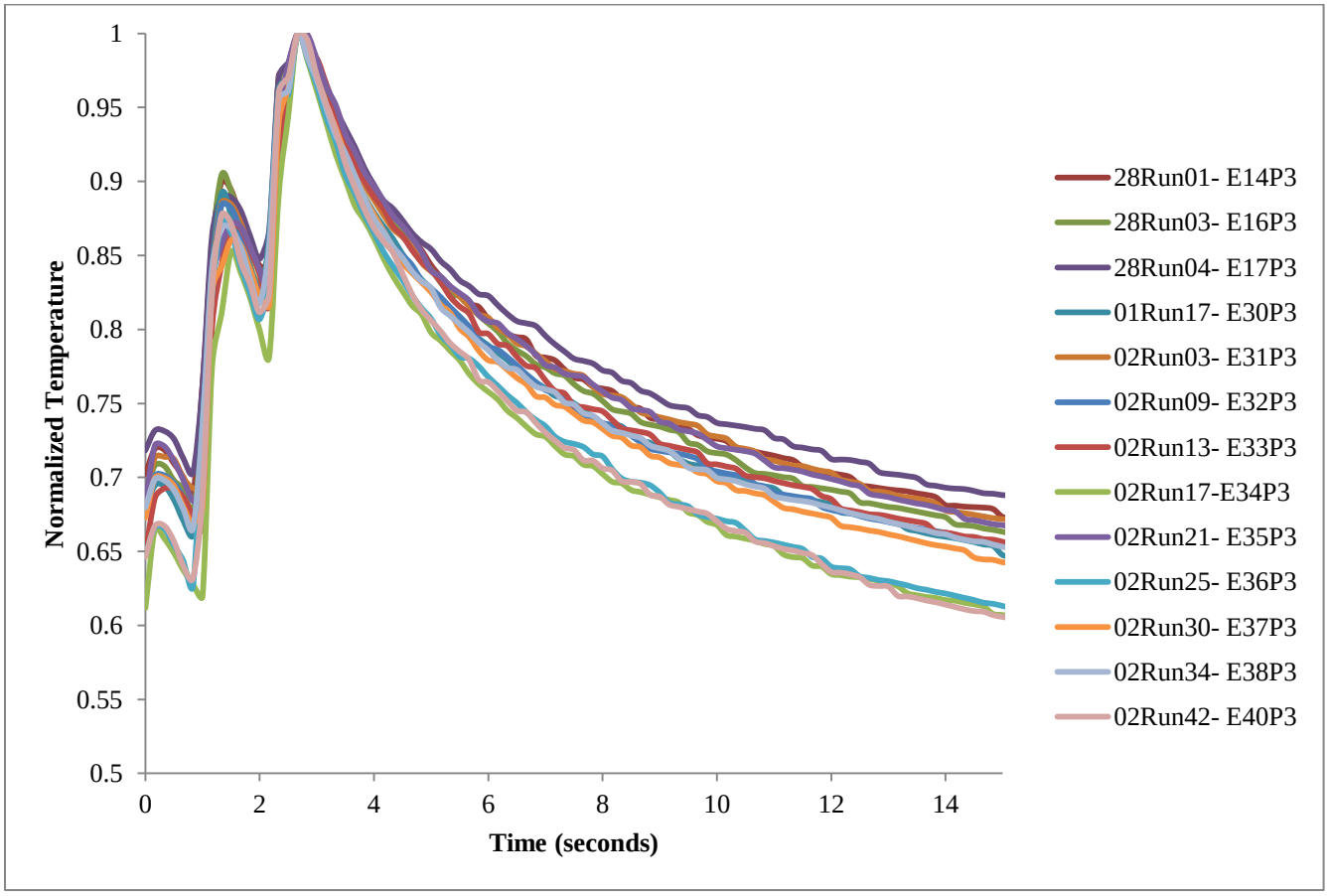


Figure 3.12. Normalized data for 3-pulse exposures for 15 separate data runs. The legend is defined in Appendix B.

An ensemble averaging 15 eye exposures was used to generate a single plot to consolidate these separate runs to a single plot. A plot displaying this averaging can be seen by referring to Figure 3.13 below. The temperature essentially returns to the baseline in about 25 seconds. Table 3.3 summarizes statistics for each of the pulse trains. Table 3.5 lists rise and fall $\Delta T/\Delta t$ rates.

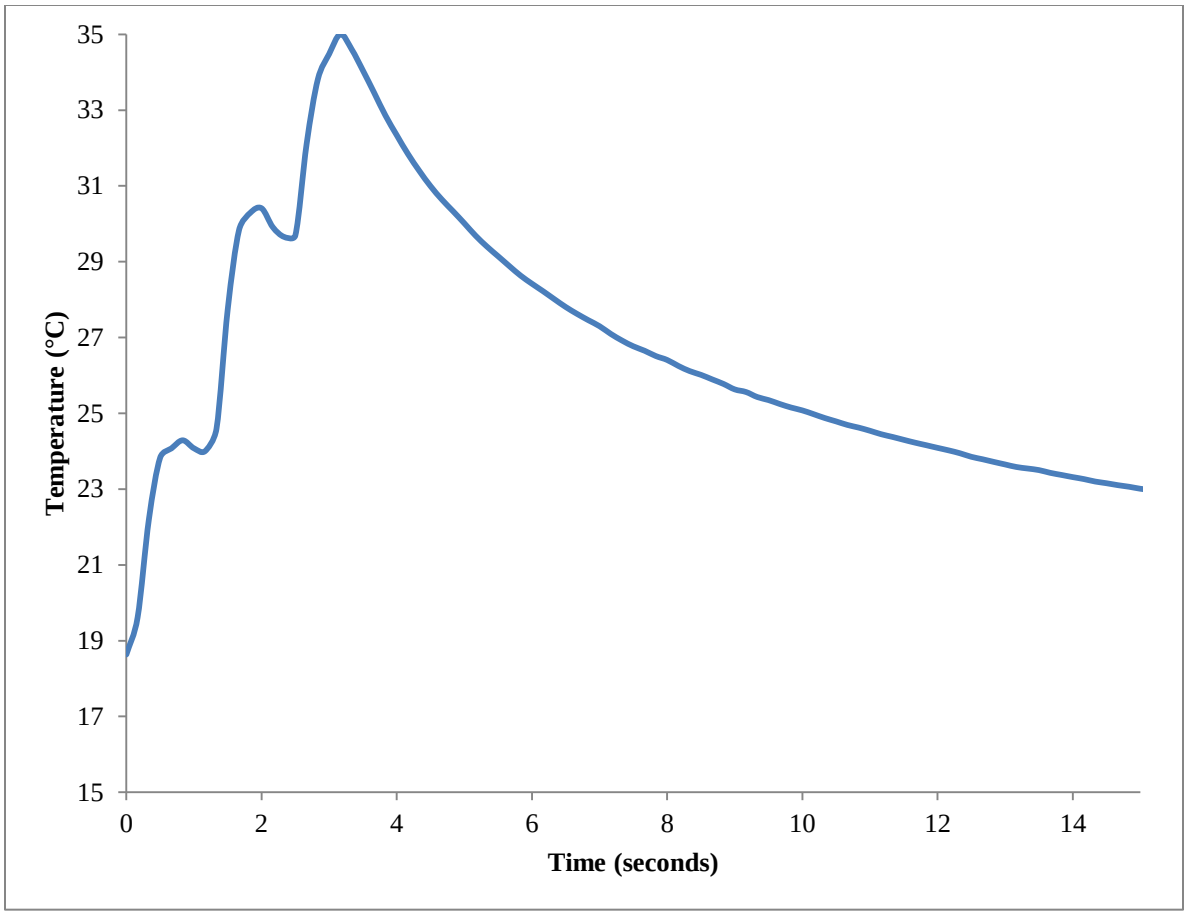


Figure 3.13. Ensemble averaging of 15 eye exposures of temperature over time with three laser pulses, incident energy at 5.83 J/cm$^2$.

### 3.6 Four Pulses

Four pulse measurements with the FLIR camera yielded an average temperature maximum of 36.0 °C and standard deviation of 1.7 °C and an average temperature increase of 17.7 °C with standard deviation of 1.5 °C. (See Table 3.3.) The overall maximum temperature was 39.6 °C with a maximum temperature increase of 19.9 °C. The total irradiance (see Table 3.1) was 5.82 J/cm$^2$ with a $\Delta T/H$ of 3.0 °C·cm$^2$/J for the first pulse, 3.6 °C·cm$^2$/J for the second pulse, 3.1 °C·cm$^2$/J for the third pulse and 2.8 °C·cm$^2$/J for the fourth pulse. (See Table 3.4.)

Normalized data was derived using the FLIR camera software to obtain the maximum temperature readings, and this data is shown in Figure 3.14. Data was collected for 14 different exposures, and Figure 3.14 shows overlaying exposures.

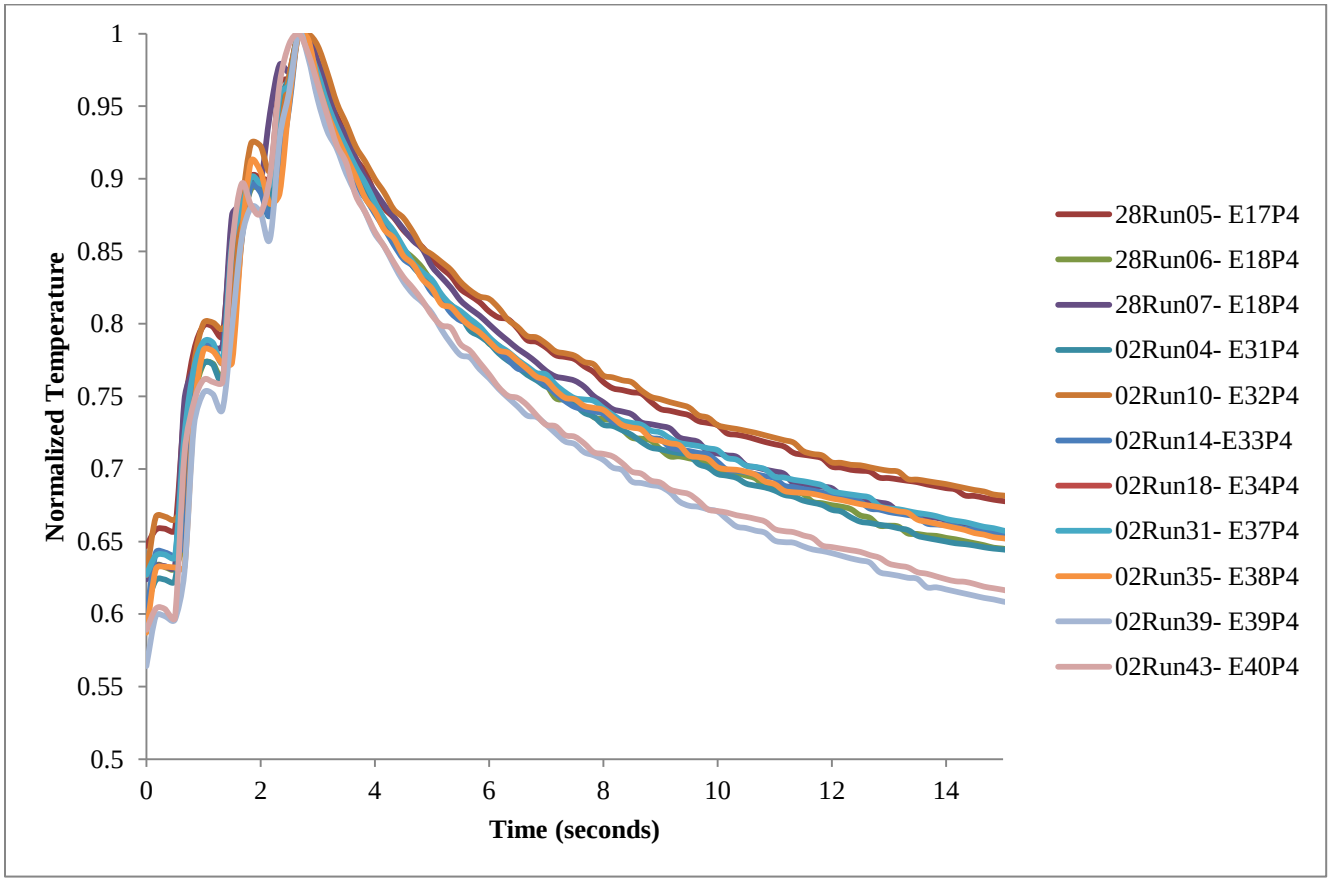


Figure 3.14. Normalized data for 4-pulse exposures for 14 separate data runs. The legend is defined in Appendix B.

An ensemble averaging 14 eye exposures was used to generate a single plot to consolidate these separate runs to a single plot. A plot displaying this averaging can be seen by referring to Figure 3.15 below. The temperature essentially returns to the starting temperature within 35 seconds. Table 3.3 summarizes statistics for each of the pulse trains. Table 3.5 lists rise and fall $\Delta T/\Delta t$ rates.

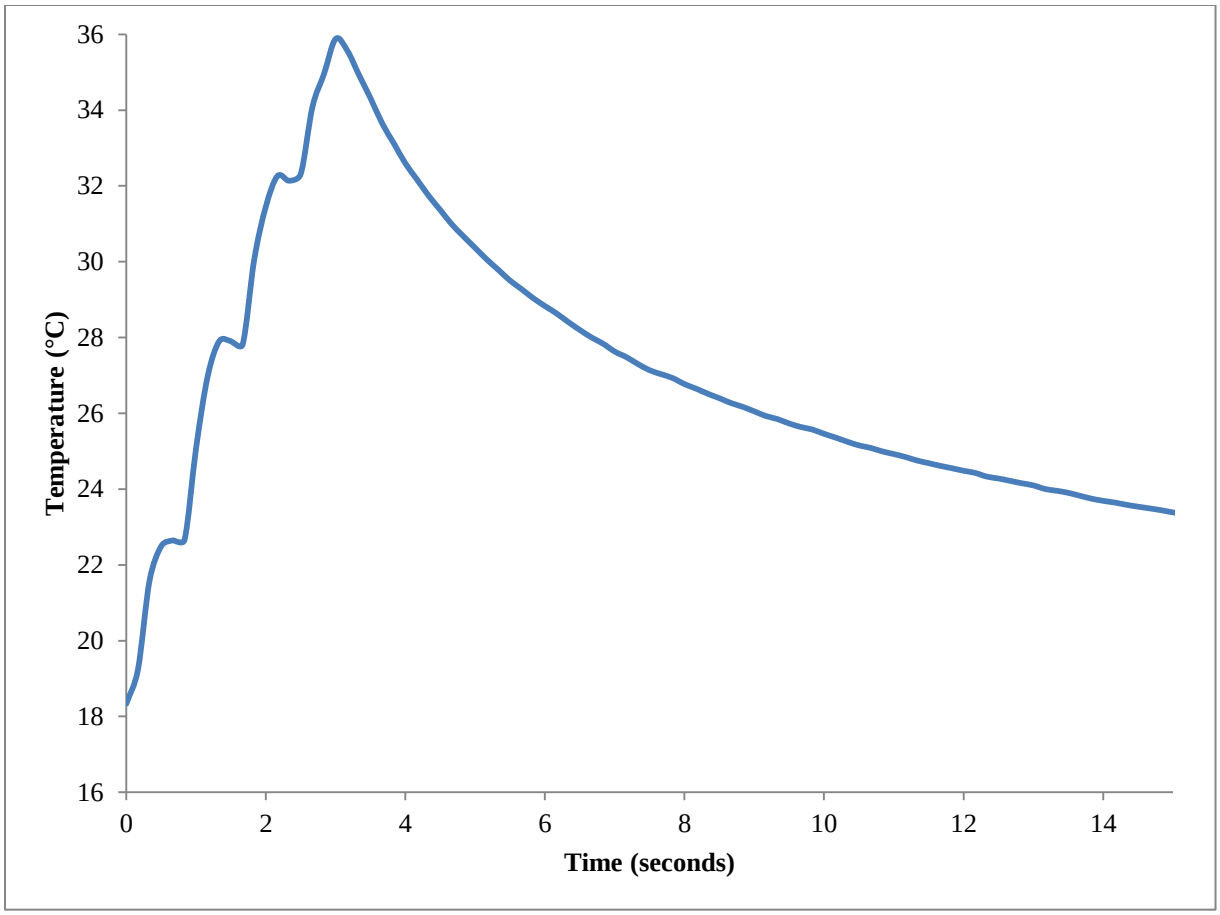


Figure 3.15. Ensemble averaging of 14 eye exposures of temperature over time with four laser pulses, incident energy at 5.82 J/cm$^2$.

# Chapter 4
# Discussion

## 4.1 Temperature Profile Discussion

Rise time is traditionally defined as the time it takes to reach 90% of maximum. Since a lag time exists between the initial laser pulse and the maximum temperature, determining the rise time between pulses can only be determined qualitatively for multiple pulse trains. Some uncertainty is due to high maintained temperatures which do not return to baseline prior to subsequent pulses that deliver additional thermal energy to the tissue. The temperature profile graphs shown in Chapter 3 demonstrate that the resulting temperature rise due to the different laser pulses. Each applied pulse is clearly identifiable in the temperature plots, so that individual peaks can be discerned. The applied laser pulses are clearly visible in the different temperature profiles despite the time lag from laser pulse to peak temperature. Table 4.1 lists times of laser pulses and the corresponding thermal pulse peak observed from the temperature measurements.

| # Pulses | Laser Pulse 1 Time | Observed Peak 1 Temperature | Laser Pulse 2 Time | Observed Peak 2 Temperature | Laser Pulse 3 Time | Observed Peak 3 Temperature | Laser Pulse 4 Time | Observed Peak 4 Temperature |
|---|---|---|---|---|---|---|---|---|
| 1 | 0.00 | 0.83 | N/A | N/A | N/A | N/A | N/A | N/A |
| 2 | 0.00 | 0.67 | 0.24 | 3.17 | N/A | N/A | N/A | N/A |
| 3 | 0.00 | 0.83 | 0.12 | 2.00 | 0.24 | 3.17 | N/A | N/A |
| 4 | 0.00 | 0.67 | 0.08 | 1.33 | 0.16 | 2.17 | 0.24 | 3.00 |

Table 4.1 Pulse arrival times of 10 ms laser pulses and observed peak temperature times. All times were measured in seconds.

The tissue heating effects are primarily delayed as a result of heat conduction and dispersion throughout the tissue.[4] The observed peak temperature occurred 0.33 seconds after the first pulse regardless of pulses in the pulse train. The follow-on observed temperature peaks were time-delayed after the time of the laser pulse (see Table 4.1) as the energy was absorbed and dispersed through the tissue. The FLIR camera response time has been examined as a factor contributing to the delay, but this was found to be negligible.[14] From Table 3.4, the $\Delta T/H$ was about 3 °C·cm$^2$/J for all pulses delivered with the exception of the two-pulse train. This two-pulse train was slightly higher at about 3.7 °C·cm$^2$/J.

### 4.2 Comparison to McCally and Bergeron[4]

Some research on temperature rise and damage threshold has been conducted in the past. Table 4.2 compares the different critical peak temperatures (CPTs), temperature data and MPE comparisons for the different pulse trains. Based on McCally and Bergeron,[4] the CPT for one pulse is 97.5 °C using a starting eye temperature of 35 °C. The *ex-vivo* rabbit corneas used in our study for a single laser pulse had a starting eye temperature of 17.6 °C. The average maximum temperature for one pulse was 25.8 °C with a temperature increase of 8.2 °C. This maximum measured temperature was far short of the calculated CPT that was 97.5 °C, with no physical damage observed on any of the 16 eyes exposed to the single pulse. The irradiance is 15.6 times greater than the calculated MPE. Much more energy can be delivered to the *ex-vivo* rabbit cornea prior to observing any damage based on the temperature difference between measured temperature and CPT. Irradiance can be increased significantly, possibly by at least an

order of magnitude before an injury manifests. Discussion of the multiple-pulse effects follows.

| Number of Pulses | 1 | 2 | 3 | 4 |
|---|---|---|---|---|
| Number of Eyes Exposed | 16 | 13 | 15 | 14 |
| CPT (°C) | 97.5 | 78.7 | 77.5 | 77.0 |
| Starting Temperature (°C) | 17.6 | 16.5 | 18.6 | 18.3 |
| Average Temperature Increase (°C) | 8.2 | 16.3 | 16.4 | 17.5 |
| Average Maximum Temperature (°C) | 25.8 | 32.8 | 35.0 | 35.9 |
| Irradiance ($J/cm^2$) - Total | 2.76 | 5.41 | 5.83 | 5.82 |
| Calculated MPE ($J/cm^2$) | 0.177 | 0.149 | 0.132 | 0.099 |
| Irradiance / MPE Multiplier | 15.6 | 36.3 | 44.2 | 58.8 |
| Observed Cornea Damage (Yes/No) | No | No | No | No |

Table 4.2 Comparing temperatures and MPE for the different pulse trains.

As depicted in Table 4.2, the McCally and Bergeron[4] CPT for two pulses was calculated at 78.7 °C. The starting temperature for eyes used in our study for two pulses was 16.5 °C, and increased by 16.3 °C to achieve an average maximum temperature ($T_{max}$) of 32.8 °C. This measured temperature is about half of the calculated CPT. The irradiance is 36.3 times greater than the calculated MPE and, as with the single pulse, no physical damage was observed on any of the 13 eyes exposed to the two pulses by a visual assessment.

Table 4.2 lists the CPT for three pulses at 77.5 °C. The average $T_{max}$ rose 16.4 °C to 35.0 °C. The irradiance is 44.2 times greater than the calculated MPE, and as with the other single and double pulses, no physical damage was observed on any of the 15 eyes exposed to the three pulses.

Table 4.2 lists the CPT for four-pulse at 77.0 °C. The average $T_{max}$ rose 17.5 °C to 35.9 °C. The irradiance is 58.8 times greater than the calculated MPE, and as with the

other pulse trains, no physical damage was observed on any of the 14 eyes exposed to the four pulses.

### 4.3 MPE recommendations

The calculated MPE for 2.01-μm pulses is significantly less than the corneal irradiance used in this study. The irradiance was kept the same for pulse trains of two, three and four to enable the comparison of pulse trains. By calculation, the MPE decreases slightly as the number of pulses goes up (from 0.18 J/cm$^2$ for one pulse to 0.14, 0.13 and 0.1 J/cm$^2$, respectively, for two, three and four pulses). The reason the single-pulse mode had a lower irradiance was because of equipment limitations of the IPG Photonics laser power output. The output was limited and could not deliver as much energy as it could for the multiple pulse configurations, so the single-pulse mode was about half of the other multiple-pulse modes. The irradiance for a single pulse was 15.6 times the MPE. Irradiances for two through four pulses ranged from 36 to 59 times the calculated MPE.

No visible damage occurred to any *ex-vivo* rabbit cornea regardless of the number of laser pulses delivered to the corneas. The ANSI MPE recommendation is defined as the intensity that is 10% of the $ED_{50}$ intensity for damage. Even though our pulses delivered between 16 to 59 times the MPE, the temperature rise resulting from the applied irradiance fell short of the CPT described by McCally and Bergeron[4] where definite visible damage is expected. The exact CPT was not determined in our study, but it appears that the MPE may be overly conservative by a factor of at least 15.

### 4.4 Future Work

We measured the *ex-vivo* rabbit corneal surface temperature for up to four laser pulses delivered within 0.25 seconds. The follow-on project should attempt to measure temperature at some variable depth into the cornea using a thermocouple system, but this process will involve freezing the corneas with a known orientation, precisely slicing the frozen sections, and measuring the distance the thermocouple was below the cornea surface with a microscope measurement system.

Future studies should focus on performing depth measurements in conjunction with the FLIR measurement system to yield three-dimensional data and aid in the understanding of how heat conduction and dispersion propagates throughout the tissue in space.

Additionally, more pulse combinations and continuous wave (CW) laser exposure experiments will add to understanding of how important the overall duration of exposure affects thermal energy transmission into *ex-vivo* rabbit corneas. Some preliminary nine-pulse and CW exposures were performed, but only three data sets were measured of each. Thus, nine-pulse and CW exposures were not statistically significant, and are not presented here.

Finally, another future study is to increase the irradiance such that CPT can be measured directly. The reason we did not attempt to achieve CPT irradiance was chiefly because the laser output used could not cover all of the different pulse trains for the power output required for the different pulse trains.

# Chapter 5
# Summary and Conclusion

## 5.1 Summary

Thermal effects corresponding to thermal energy absorption in the *ex-vivo* rabbit cornea using laser power levels with millisecond-scale pulses were measured. Past research has shown that the cornea is the part of the eye most susceptible to damage from a laser operating at the 2.01-μm wavelength.

Current laser safety standards for multiple-pulse lasers are based primarily on modeling and the results of single-pulse studies. An infrared thermal camera employing microbolometer detectors captured surface temperature rises resulting from laser pulses on an *ex-vivo* rabbit cornea. Thermal measurements were taken with single 10-ms pulses as well as two-, three-, and four-pulse sequences while holding the total energy delivered constant for the two- through four-pulse train measurements. An average temperature increase of 8.3 °C was observed with the single pulse at 2.8 J/cm$^2$/pulse irradiance. For two pulses, an average temperature increase of 10.0 °C was observed for 2.7 J/cm$^2$/pulse irradiance. For three pulses, an average temperature increase of 5.8 °C was observed for 1.9 J/cm$^2$/pulse irradiance. For four pulses, an average temperature increase of 4.4 °C was observed for 1.5 J/cm$^2$/pulse irradiance.

This study also compared temperature change measurements to theoretical peak temperature calculations. Comparisons were made to the McCally and Bergeron[4] study done investigating the threshold peak temperatures they used to fit by a modified critical peak temperature (CPT) model. It was found that measured temperatures did not approach the CPT, and no tissue damage was observed in any *ex-vivo* rabbit cornea. The measured-to-calculated MPE ratio multiplier for each scenario increased from a factor of 16 for the single-pulse measurement to 36 for two pulses to 44 for three pulses and to 59 for four pulses.

As discussed in Chapter 4, suggested follow-on studies include to measure temperatures with a thermocouple to capture temperatures at a corresponding depth from cornea surface and to conduct temperature measurements to find when damage occurs and at what temperature. Then, a comparison of thermocouple measurements to the critical peak temperatures should be studied as outlined in the 2003 McCally and Bargeron paper.

## 5.2 Conclusion

Direct comparisons to the McCally model could not be performed since the laser output was insufficient to cause tissue damage to the cornea. More experimentation at higher irradiances can determine precisely when damage occurs to validate the CPTs postulated in the McCally study.

The ANSI MPE for single-pulse and two-pulse through four-pulse sequences is overly restrictive. No corneal damage was observed at levels ranging from 16 to 59 times the calculated MPE for pulse trains of one to four, respectively. The increase of the MPE

by a factor of ten would still provide sufficient protection from corneal damage resulting from laser exposure at this wavelength. It is recommended that the 2.01-μm laser MPE be investigated to determine if a revision of the standard is warranted.

## References


[1] Occupational Safety and Health Administration, "Guidelines for laser safety and hazard assessment," Report STD 01-05-001 [Pub 8-1-7], (1991)

[2] American National Standards Institute, "American national standard for safe use of lasers," Report No. ANSI Z136.1-2007, (2007)

[3] N.A. Peppers, A. Vassiliadia, K.G. Dedrick, H. Chang, R.R. Peabody, H. Rose, and H.C. Zweng, "Corneal Damage Thresholds for $CO_2$ Laser Radiation," Applied Optics **8** (2), 377-381 (1969)

[4] M. L. Wolbarsht, "Laser Applications in Medicine and Biology, Volume 1," Plenum Press, New York (1971)

[5] R. L. McCally and C. B. Bargeron, "Corneal Epithelial Injury Thresholds for Multiple-Pulse Exposures to Tm:YAG Laser Radiation at 2.02 μm," Health Physics **85**(4), 420-427 (2003)

[6] J. A. Curcio and C. C. Petty, "The near infrared absorption spectrum of liquid water," Journal of the Optical Society of America **41** (5), 302-304 (1951)

[7] M. R. Querry and G. M. Hale, "Optical-constants of water in 200-nm to 0.2-mm wavelength region," Journal of the Optical Society of America **62** (11), 1381-1381 (1972)

[8] MH Niemz, "Laser-tissue interactions: Fundamentals and applications," Springer Verlag, (2003)

[9] B. Chen, H. W. Kang, S. L. Thomsen, and A. J. Welch, "Modeling thermal response of skin to 2000 nm laser irradiation," Lasers in Surgery and Medicine, 274 (2006)

[10] D. C. Hanna, I. R. Perry, J. R. Lincoln, and J. E. Townsend, "A 1-watt thulium doped CW fibre laser operating at 2 μm," Optics Communications 80 (1), 52-56 (1990)

[11] S. D. Jackson and T. A. King, "High-power diode-cladding-pumped Tm-doped silica fiber laser," Optics Letters **23** (18), 1462-1464 (1998)

[12] D. K. Sardar, G. Y. Swanland, R. M. Yow, R. J. Thomas, and A. T. Tsin, "Optical Properties of Ocular Tissues in the Near Infrared Region," Lasers Med Sci 22: 46-52 (2007)

[13] R. L. McCally, R. A. Farrell, and C. B. Bargeron, "Cornea epithelial damage thresholds in rabbits exposed to Tm-YAG laser-radiation at 2.02 μm," Lasers in Surgery and Medicine 12 (6), 598-603 (1992)

[14] D.N. Schaaf, "Skin Tissue Optical and Thermal Reactions to Pulse Sequences of Thulium Yttrium Aluminum Garnet Laser Irradiation," PhD Dissertation, Colorado State University (2010)

[15] D. Dugan, "Determination of Sensation Thresholds From Single 10 ms Pulses Of 2.01 μm Laser Light Incident On Human Skin," Master's Thesis, Colorado State University (2009)

[16] P. J. Shayler, "Laser-beam distribution in focal region," Applied Optics 17 (17), 2673-2674 (1978)

[17] A.S. Sedra and K.C. Smith, " Microelectronic Circuits, Third Edition," Saunders College Publishing (1982)

# Appendix A

This appendix contains specifications and engineering drawings of equipment used to conduct this study. Additionally, experimental setup directions are included to facilitate any follow-up study that may occur.

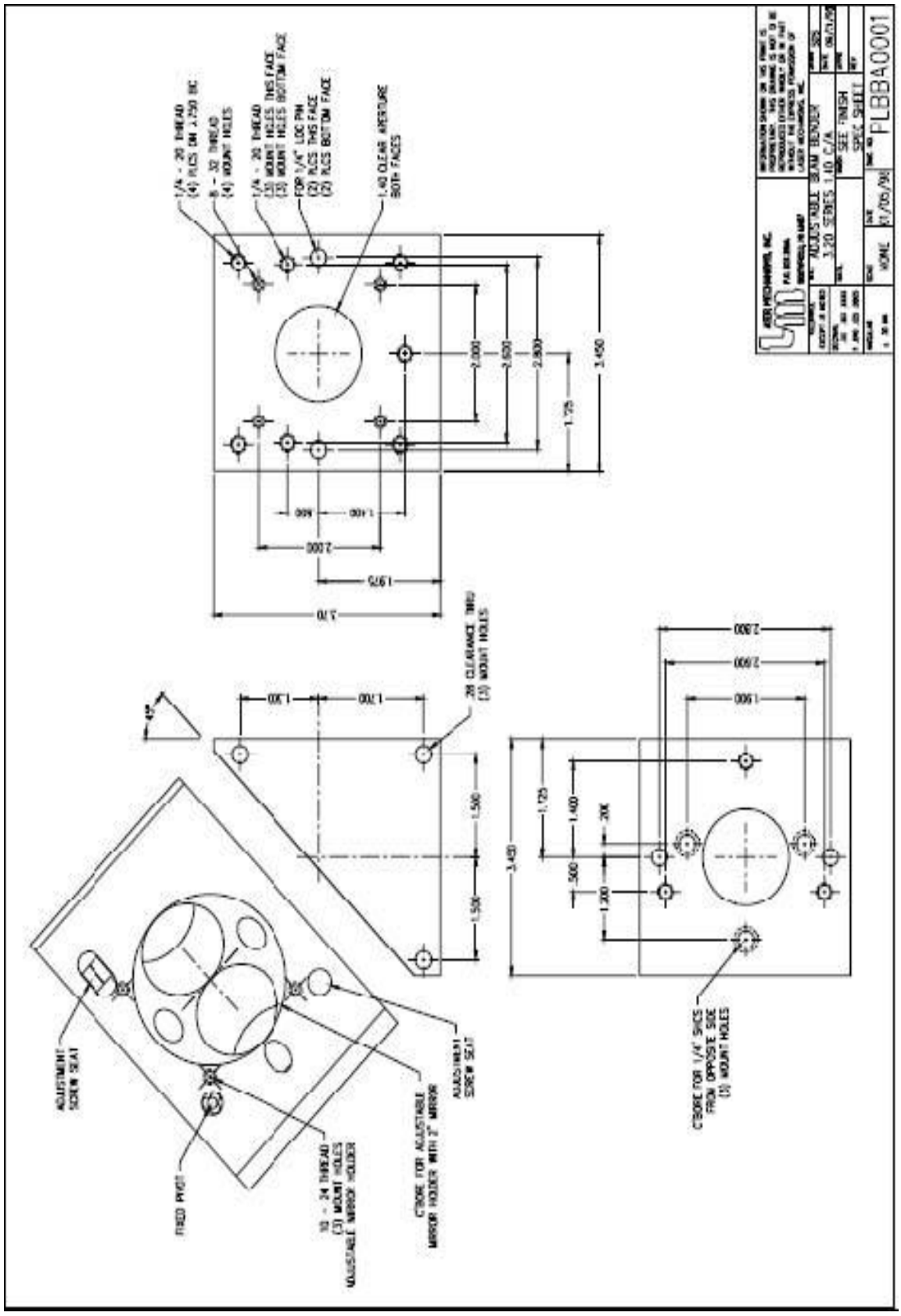
FLBBA0001

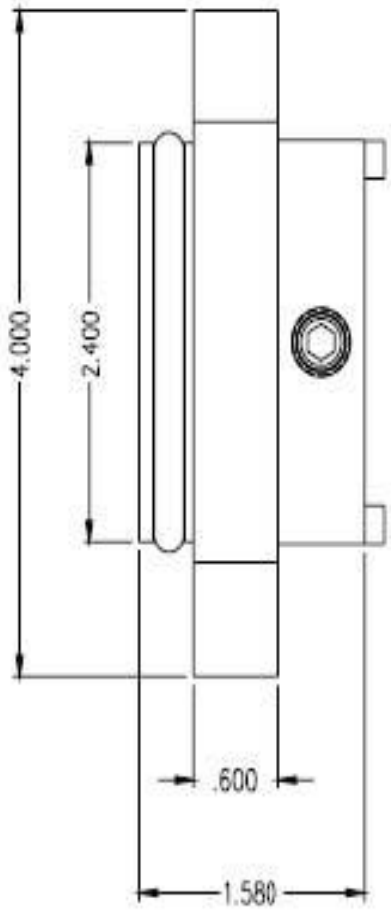


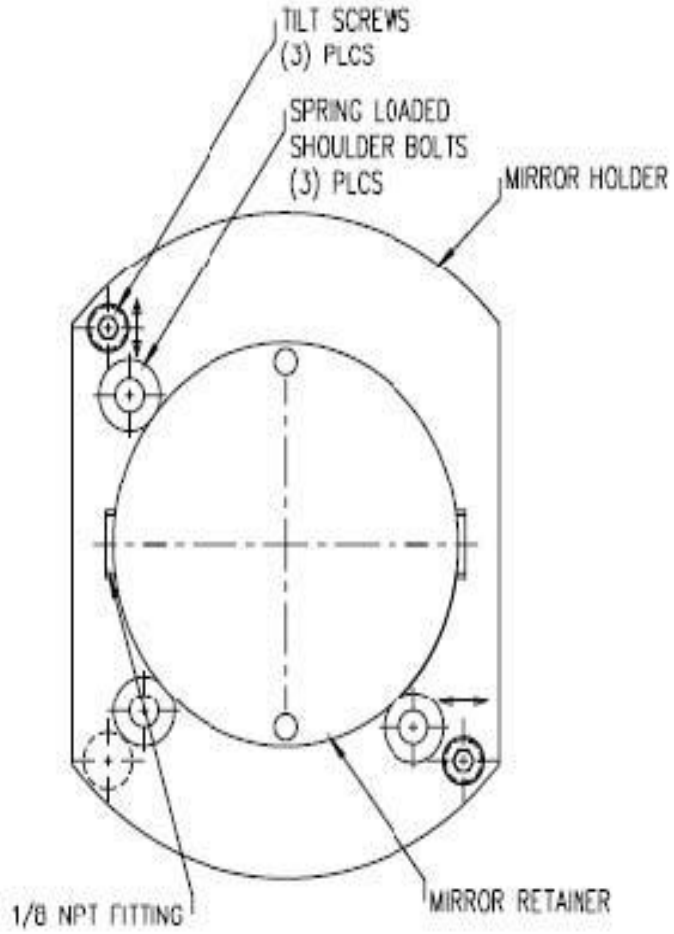


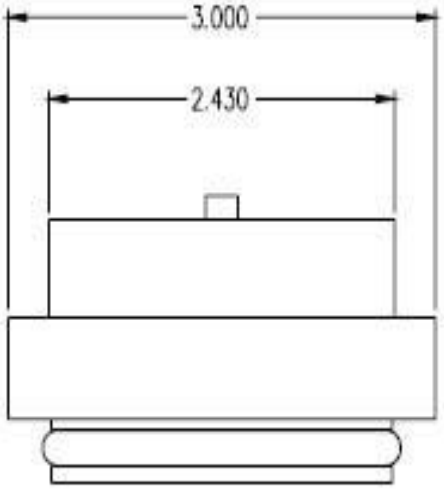


| | | | |
|---|---|---|---|
| | ADJUSTABLE MIRROR HOLDER 1" MIRROR | | |
| | | SEE FINISH SPEC SHEET | |
| | NONE | 07/29/99 | PLAMH0018 |

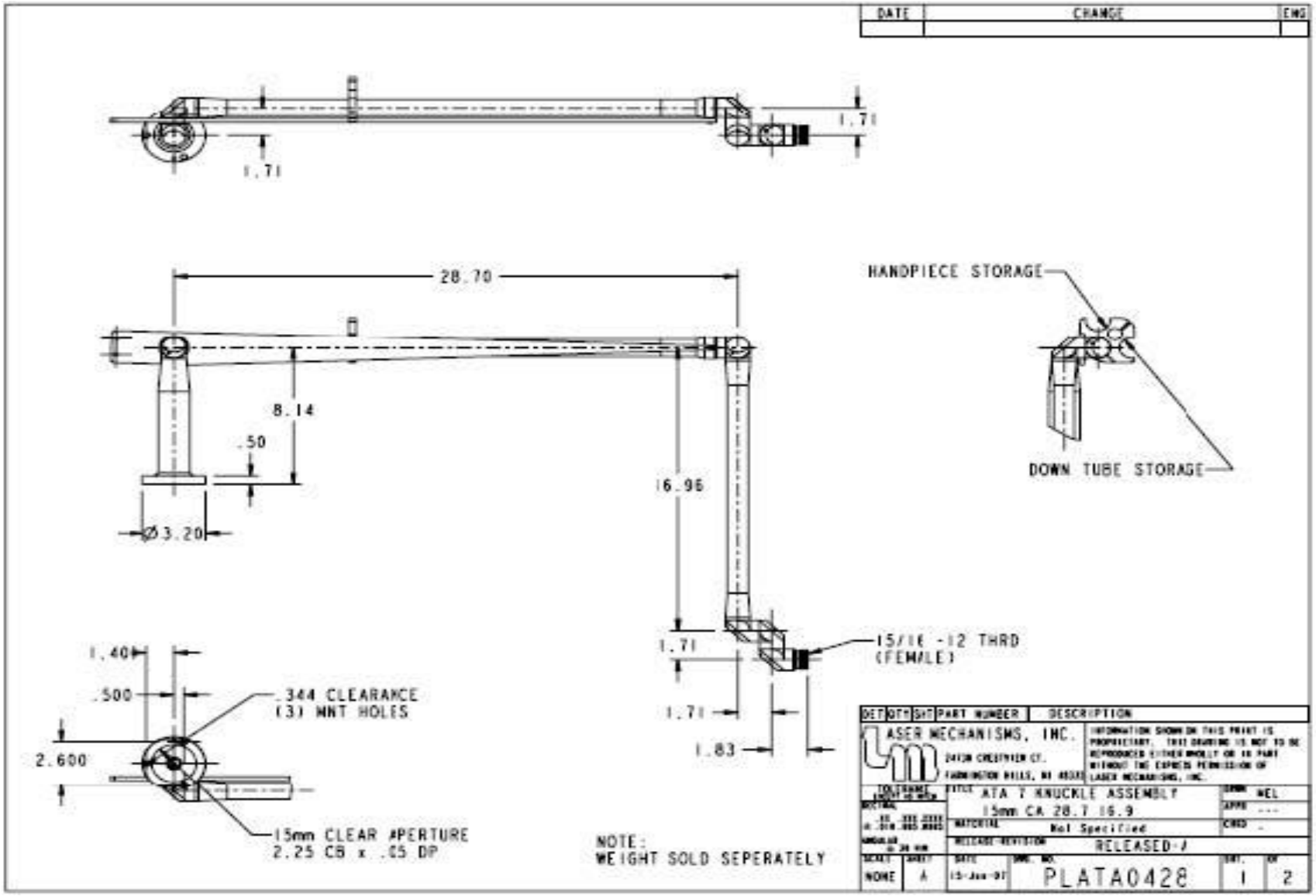
DATE
CHANGE
ENG
1.71
1.71
28.70
8.14
.50
Ø3.20
16.96
1.71
1.71
1.83
15/16 -12 THRD
(FEMALE)
HANDPIECE STORAGE
DOWN TUBE STORAGE
1.40
.500
.344 CLEARANCE
(3) MNT HOLES
2.600
15mm CLEAR APERTURE
2.25 CB x .05 DP
NOTE:
WEIGHT SOLD SEPERATELY
DET
QTY
SHT
PART NUMBER
DESCRIPTION
LASER MECHANISMS, INC.
INFORMATION SHOWN ON THIS PRINT IS PROPRIETARY. THIS DRAWING IS NOT TO BE REPRODUCED EITHER WHOLLY OR IN PART WITHOUT THE EXPRESS PERMISSION OF LASER MECHANISMS, INC.
TITLE
ATA T KNUCKLE ASSEMBLY
15mm CA 28.7 16.9
DRWN MEL
APPR ---
CHKD -
MATERIAL
Not Specified
RELEASE-REVISION
RELEASED-J
SCALE
NONE
SHEET
A
DATE
15-Jun-01
DWG. NO.
PLATA0428
REV.
1
OF
2

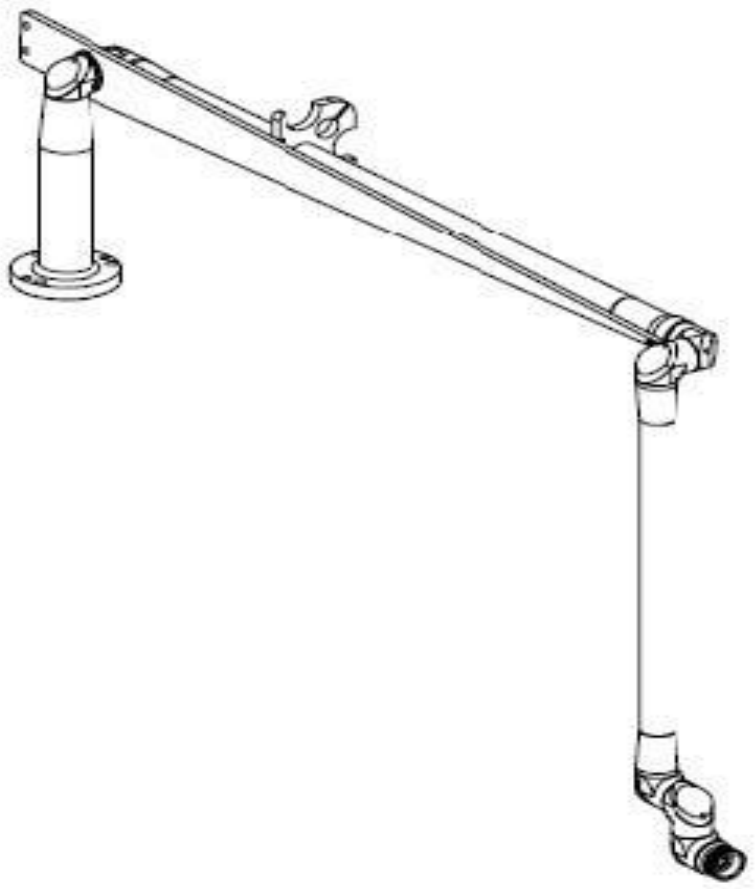

| DATE | CHANGE | ENG |
|---|---|---|
| | | |

| ITEM | QTY | SHT | PART NUMBER | DESCRIPTION |
|---|---|---|---|---|
| 16 | 1 | | FLKMC1001 | KNUCKLE CAP ASSEMBLY 1.25 SER. |
| 15 | 1 | | FLATT0265 | TUBE ASSY BEA 1.05 3/4 QL 15.6 |
| 14 | 1 | | FLATT0091 | TUBE ASSY w/BEAUTY |
| 13 | 1 | | FLATB0055 | ONE PIECE BASE 15mm 1.5 |
| 12 | 1 | | FLAFK1006 | KNUCKLE ASSEMBLY 1.25 CANT. |
| 11 | 1 | | FLAFK1005 | KNUCKLE ASSEMBLY 1.25 SER. |
| 10 | 5 | | FLAFK1004 | KNUCKLE ASSEMBLY 1.25 SER. |
| 9 | 1 | | FLAAC0007 | ART ARM CLAMP |
| 8 | 3 | | L04365A | WASHER |
| 7 | 7 | | L00900C | SHIM |
| 6 | 1 | | L00842S | CANTILEVER NO OFFSET |
| 5 | 1 | | L00C99M | HANDPIECE 15/16-12 |
| 4 | 1 | | L04365 | WASHER |
| 3 | 1 | | L00867 | BEAUTY RING |
| 2 | 1 | | C05297 | BHCS 6-32 x 7/16 SHDR S.S. |
| 1 | 1 | | C00662 | SNAP RING |

LASER MECHANISMS, INC.
34124 CRESTVIEW CT.
FARMINGTON HILLS, MI 48331



TOLERANCE UNLESS OTHERWISE SPECIFIED
.XX ±.010 .XXX ±.005
ANGULAR ±1°

TITLE: ATA T KNUCKLE ASSEMBLY 15mm CA 28.7 16.9
MATERIAL: Not Specified
RELEASE REVISION: RELEASED-A
DRWN: NEL
DATE: ---
CHD: ---

SCALE: NONE | SHEET: A | DATE: 15-Jun-07 | DWG. NO. PLATA0428 | SH. 2 | OF 2

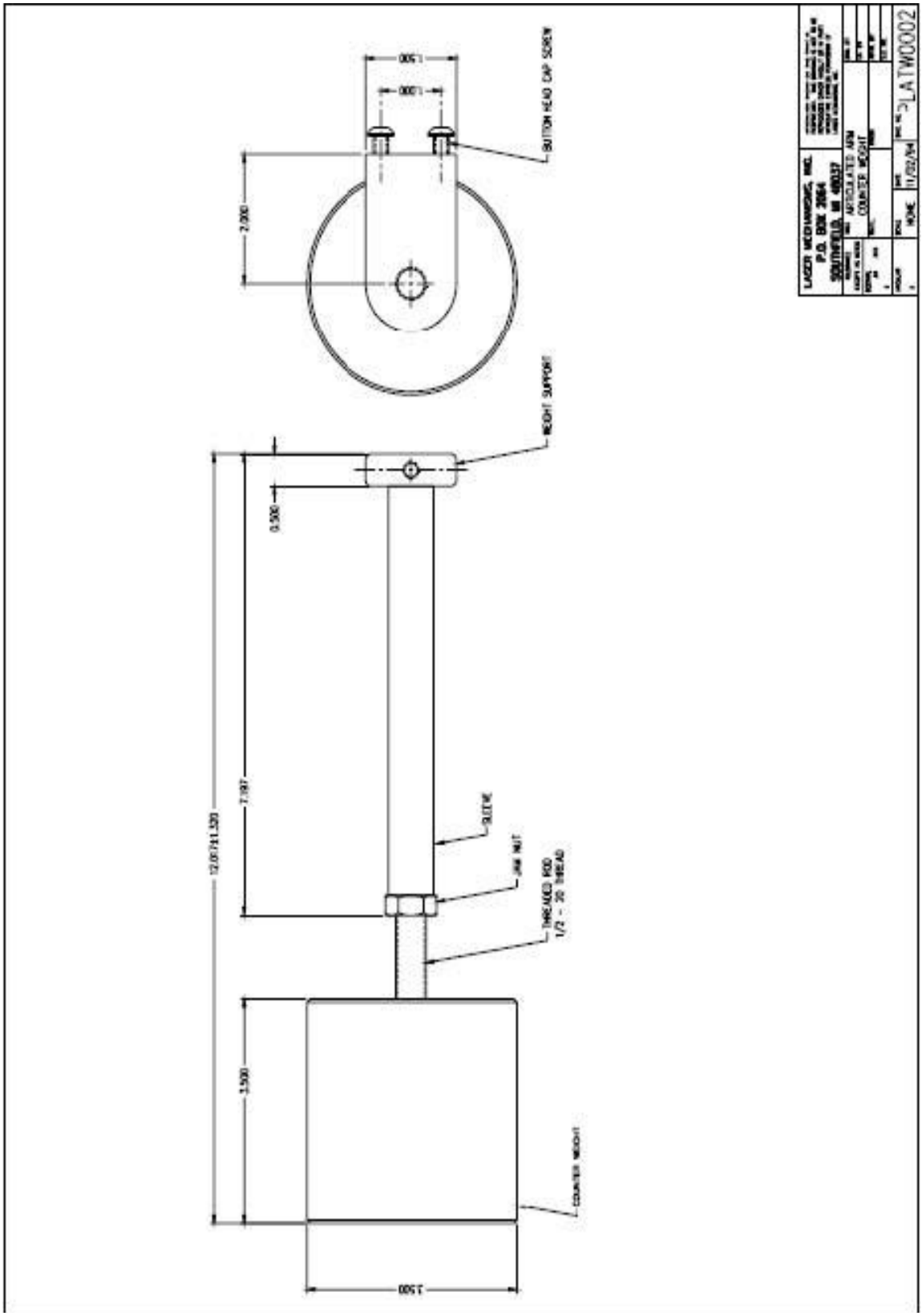
LATW0002

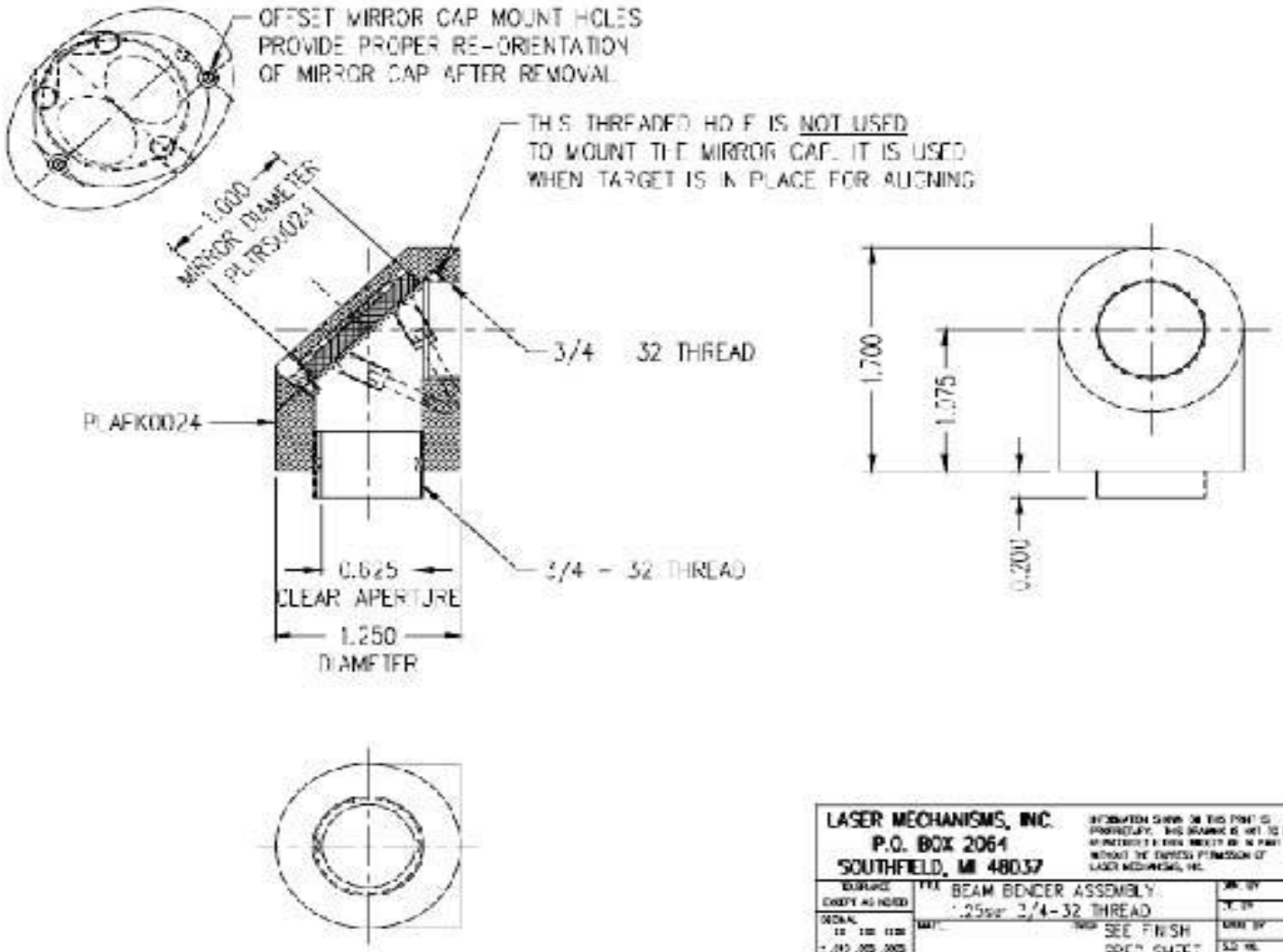
OFFSET MIRROR CAP MOUNT HOLES
PROVIDE PROPER RE-ORIENTATION
OF MIRROR CAP AFTER REMOVAL
THIS THREADED HOLE IS NOT USED
TO MOUNT THE MIRROR CAP. IT IS USED
WHEN TARGET IS IN PLACE FOR ALIGNING
1.000
MIRROR DIAMETER
PLTR3A024
3/4 32 THREAD
PLAFK0024
3/4 - 32 THREAD
0.625
CLEAR APERTURE
1.250
DIAMETER
1.700
1.375
0.200
LASER MECHANISMS, INC.
P.O. BOX 2064
SOUTHFIELD, MI 48037
BEAM BENDER ASSEMBLY
1.25ø 3/4-32 THREAD
SEE FINISH
SPEC SHEET
SCALE
NONE
DATE
06/20/95
BBA0041A

# Standard Operating Procedure

TLR-50-2010
Thulium Fiber Laser

**Frequency Generator**

1) Turn on both frequency generators

2) Plug the BNC connector from the laser button on the arm into the trigger input on the back of the "Master" generator

3) Plug the output from the Master into the BNC trigger on the "Slave"

4) Plug the output from the Slave to the BNC T connector on the Back of the Laser

5) The Slave's settings are as follows:

| | |
|---|---|
| Frequency | 50 Hz |
| Waveform | Square |
| VPP | 2.5V |
| Offset | 1.25 V |
| Pulses | 1 |

6) The Master's settings are:

| | |
|---|---|
| Waveform | Square |
| VPP | 2.5 V |
| Offset | 1.25 V |

7) With the frequency and number of pulses varying use the following values:

| Frequency (Hz) | Pulses |
|---|---|
| 4.166666 | 2 |
| 8.333333 | 3 |
| 12.5 | 4 |

8) Each row in the above table corresponds to one day. That is, you'll need to set the number of pulses in a train to 3, and also set the frequency to 8.333333Hz. Also, completely set the decimals don't stop at 8.33 for example to ensure no round-off error impacts the number of pulses to fit into a 250 ms window.

9) Refer to the HP 33120A User Guide to go through the menu systems, and verify on an oscilloscope that the pulse train is getting the correct control signal. To set the burst mode, use the MODulation MENU, select 4: BURST CNT, set to the number of pulses desired within the pulse train. Set the signal generator for trigger mode.

## Appendix B

This appendix defines the naming structure used to collect data. The structure was composed as follows: *dd*Run*xx*-E*yy*Pz. The variables are defined as follows. The *dd* represents the date the measurement was taken. The dates were 26 May, 28 May, 1 Jun and 2 Jun, so the set *dd* is {26, 28, 01, 02}. The variable *xx* is comprised of the set {1, 2, 3, …, 51} to represent the sequence of data (runs) collected in a day. Please note that about six data runs were eliminated due to a technical problem such as a slow camera response that caught the temperature profile too late or the laser that did not turn on as commanded. The variable *yy* after E represents the number of the *ex-vivo* eye's cornea used. In all, 42 rabbit eyes were shipped from Pel-Freeze, so this set comprises of {1, 2, 3, …, 42}. Finally, the variable *z* following the letter P represents how many pulses {1, 2, 3, 4} were delivered to the *ex-vivo* rabbit cornea.

The following chart details the described structure.

| Data Name | Data Defined |
|---|---|
| 26Run04- E03P1 | 26 May 2010, Run 4, Eye 3, 1 Pulse |
| 26Run05- E03P1 | 26 May 2010, Run 4, Eye 3, 1 Pulse |
| 26Run06- E04P1 | 26 May 2010, Run 6, Eye 4, 1 Pulse |
| 26Run08- E06P1 | 26 May 2010, Run 8, Eye 6, 1 Pulse |
| 26Run09- E07P1 | 26 May 2010, Run 9, Eye 7, 1 Pulse |
| 28Run01- E14P3 | 28 May 2010, Run 1, Eye 14, 3 Pulses |
| 28Run03- E16P3 | 28 May 2010, Run 3, Eye 16, 3 Pulses |
| 28Run04- E17P3 | 28 May 2010, Run 4, Eye 17, 3 Pulses |
| 28Run05- E17P4 | 28 May 2010, Run 5, Eye 17, 4 Pulses |
| 28Run06- E18P4 | 28 May 2010, Run 6, Eye 18, 4 Pulses |
| 28Run07- E18P4 | 28 May 2010, Run 7, Eye 18, 4 Pulses |
| 01Run10- E26P1 | 1 June 2010, Run 10, Eye 26, 1 Pulse |
| 01Run12- E27P1 | 1 June 2010, Run 12, Eye 27, 1 Pulse |
| 01Run15- E30P1 | 1 June 2010, Run 15, Eye 30, 1 Pulse |
| 01Run16- E30P2 | 1 June 2010, Run 16, Eye 30, 2 Pulses |
| 01Run17- E30P3 | 1 June 2010, Run 17, Eye 30, 3 Pulses |
| 02Run01- E31P1 | 2 June 2010, Run 1, Eye 31, 1 Pulse |
| 02Run02- E31P2 | 2 June 2010, Run 2, Eye 31, 2 Pulses |
| 02Run03- E31P3 | 2 June 2010, Run 3, Eye 31, 3 Pulses |
| 02Run04- E31P4 | 2 June 2010, Run 4, Eye 31, 4 Pulses |
| 02Run08- E32P2 | 2 June 2010, Run 8, Eye 32, 2 Pulses |
| 02Run09- E32P3 | 2 June 2010, Run 9, Eye 32, 3 Pulses |
| 02Run10- E32P4 | 2 June 2010, Run 10, Eye 32, 4 Pulses |
| 02Run11- E33P1 | 2 June 2010, Run 11, Eye 33, 1 Pulse |
| 02Run12- E33P2 | 2 June 2010, Run 12, Eye 33, 2 Pulses |

| | |
|---|---|
| 02Run13- E33P3 | 2 June 2010, Run 13, Eye 33, 3 Pulses |
| 02Run14-E33P4 | 2 June 2010, Run 14, Eye 33, 4 Pulses |
| 02Run15- E34P1 | 2 June 2010, Run 15, Eye 34, 1 Pulse |
| 02Run16- E34P2 | 2 June 2010, Run 16, Eye 34, 2 Pulses |
| 02Run17-E34P3 | 2 June 2010, Run 17, Eye 34, 3 Pulses |
| **Data Name** | **Data Defined** |
| 02Run18- E34P4 | 2 June 2010, Run 18, Eye 34, 4 Pulses |
| 02Run20- E35P2 | 2 June 2010, Run 20, Eye 35, 2 Pulses |
| 02Run21- E35P3 | 2 June 2010, Run 21, Eye 35, 3 Pulses |
| 02Run22- E35P4 | 2 June 2010, Run 22, Eye 35, 4 Pulses |
| 02Run23- E36P1 | 2 June 2010, Run 23, Eye 36, 1 Pulse |
| 02Run24- E36P2 | 2 June 2010, Run 24, Eye 36, 2 Pulses |
| 02Run25- E36P3 | 2 June 2010, Run 25, Eye 36, 3 Pulses |
| 02Run28- E37P1 | 2 June 2010, Run 28, Eye 37, 1 Pulse |
| 02Run29- E37P2 | 2 June 2010, Run 29, Eye 37, 2 Pulses |
| 02Run30- E37P3 | 2 June 2010, Run 30, Eye 37, 3 Pulses |
| 02Run31- E37P4 | 2 June 2010, Run 31, Eye 37, 4 Pulses |
| 02Run33- E38P2 | 2 June 2010, Run 33, Eye 38, 2 Pulses |
| 02Run34- E38P3 | 2 June 2010, Run 34, Eye 38, 3 Pulses |
| 02Run35- E38P4 | 2 June 2010, Run 35, Eye 38, 4 Pulses |
| 02Run37- E39P2 | 2 June 2010, Run 37, Eye 39, 2 Pulses |
| 02Run39- E39P4 | 2 June 2010, Run 39, Eye 39, 4 Pulses |
| 02Run40- E40P1 | 2 June 2010, Run 40, Eye 40, 1 Pulse |
| 02Run41- E40P2 | 2 June 2010, Run 41, Eye 40, 2 Pulses |
| 02Run42- E40P3 | 2 June 2010, Run 42, Eye 40, 3 Pulses |
| 02Run43- E40P4 | 2 June 2010, Run 43, Eye 40, 4 Pulses |
| 02Run44- E41P1 | 2 June 2010, Run 44, Eye 41, 1 Pulse |
| 02Run45- E41P2 | 2 June 2010, Run 45, Eye 41, 2 Pulses |
| 02Run46- E41P3 | 2 June 2010, Run 46, Eye 41, 3 Pulses |
| 02Run47- E41P4 | 2 June 2010, Run 47, Eye 41, 4 Pulses |
| 02Run48- E42P1 | 2 June 2010, Run 48, Eye 42, 1 Pulse |
| 02Run49- E42P2 | 2 June 2010, Run 49, Eye 42, 2 Pulses |
| 02Run50- E42P3 | 2 June 2010, Run 50, Eye 42, 3 Pulses |
| 02Run51- E42P4 | 2 June 2010, Run 51, Eye 42, 4 Pulses |